

Defect–Defect Correlation Functions, Generic Scale Invariance, and the Complex Ginzburg–Landau Equation

Bruce W. Roberts, Eberhard Bodenschatz, and James P. Sethna

Laboratory of Atomic and Solid–State Physics,
Cornell University,
Ithaca, NY 14853–2501.

Keywords: Complex Ginzburg–Landau Equation, Topological Defects, Generic Scale Invariance

PACS: 05.45.+b,47.20.Tg

Abstract

Motivated by the idea of developing a “hydrodynamic” description of spatiotemporal chaos, we have investigated the defect–defect correlation functions in the defect turbulence regime of the two–dimensional, anisotropic complex Ginzburg–Landau equation. We compare our results with the predictions of generic scale invariance. Using the topological nature of the defects, we prove that defect–defect correlations cannot decay as slowly as predicted by generic scale invariance. We also present results on the fluctuations of the amplitude field A .

1 Introduction

Chaos is the name given to intrinsic random behavior arising in a deterministic system [1]. The simplest forms of chaos occur in systems of three or more coupled ordinary differential equations and in discrete mappings. A great deal is known about such systems with a small number of degrees of freedom displaying “temporal chaos”, where the structure of the phase space can be analyzed in detail. Spatially extended systems with many interacting degrees of freedom exhibit “spatiotemporal chaos” [2], in which the chaotic fluctuations occur on spatial scales as well as in time. Spatiotemporal chaos has also been called “weak turbulence”, “defect chaos”, and “defect turbulence”. (This is to be distinguished from fully developed turbulence, which typically occurs for increasing driving but fixed size L , while spatiotemporal chaos occurs for fixed large driving but increasing L .) There have been a number of approaches used in attempting to understand spatiotemporal chaos: partial differential equations, coupled ordinary differential equations (in which space is discretized), coupled map lattices [3] (in which space and time are discretized), and cellular automata (in which space, time, and dependent variable are discretized). For large systems, we may hope to use a statistical description of the chaotic states, borrowing concepts from equilibrium statistical mechanics. We wish to find simple reduced descriptions, emphasizing the collective behavior of many chaotic degrees of freedom, analogous to the reduced long-wavelength description provided by thermodynamics and hydrodynamics for equilibrium systems [4, 5, 6, 7, 8, 9].

Typically, spatiotemporal chaos appears in nonequilibrium pattern-forming systems slightly above their threshold of instability [10]. The study of spatiotemporal chaos has been advanced by the development of experimental systems which are precisely controlled and have a large aspect ratio [11, 12, 13, 14, 15, 16, 17, 18, 19]. Such systems have large statistically homogeneous regions relatively free from boundary effects. A key question to address is whether such regions can be described in terms of hydrodynamic-like theories, focusing on collective behaviors and long-wavelength descriptions. We wish to address an aspect of this question by considering the coherent structures known as topological defects (or spirals or vortices) in a system that exhibits spatiotemporal chaos: the complex Ginzburg–Landau equation [20, 21, 22, 23, 24]. This equation describes the slowly varying amplitude and phase in an extended system which undergoes a supercritical Hopf bifurcation to an oscillating and spatially uniform or oscillatory and spatially periodic state. The equation exhibits many interesting patterns, but we will restrict our investigation to the Benjamin–Feir unstable (or defect turbulent) regime [25], in which topological defects occur in the context of spatiotemporal chaos. Other systems, such as Rayleigh–Bénard convection [11, 12, 13], electrohydrodynamic convection in liquid crystals [15, 16, 17, 26, 27], capillary ripples [18], cardiac tissue [28], chemical reactions [29], and wide aperture lasers [19, 30], can exhibit similar defect-turbulent behavior. Here, we will examine the defect–defect correlation functions and relate them to the ideas of generic scale invariance, which is a theory for describing nonequilibrium systems with conservation laws. We will prove that the generic predictions cannot be correct for topological defect correlations. Finally, we will see that our numerical results do not agree with the predictions of generic scale invariance [31, 32, 33, 34, 35].

This paper is organized as follows. In Section 2 we discuss briefly the complex Ginzburg–Landau equation. The numerical technique that we use to solve this equation is discussed in Section 3. Some interesting results that don’t depend solely upon the defects in the

system are presented in Section 4. In Section 5 we briefly describe the ideas behind generic scale invariance, and relate these ideas to the topological defects in the complex Ginzburg–Landau equation. Constraints on the behavior of the defects due to their topological nature are discussed in Section 6. The predictions of generic scale invariance, as well as that from the constraints, are compared with numerical results in Section 7. Finally, we present our conclusions in Section 8.

2 The Complex Ginzburg–Landau Equation

Perturbative analyses of microscopic equations for various pattern-forming systems yield complex partial differential equations which go under the name “amplitude equations”. Considered in their own right as model dynamical systems which do not necessarily describe any real physical system, these equations are referred to as Ginzburg–Landau models. It is important to note the role of these Ginzburg–Landau equations as model equations. Many properties of nonequilibrium systems are encountered in these equations. Many hard problems, such as the existence and interaction of defects and coherent structures, or the appearance of chaos, can be profitably addressed in the simple framework provided by these equations. However, these equations provide a quantitative description of real experiments valid only in a small region near the transition threshold for a pattern. Far from threshold, only the phase of the complex field survives as a slow degree of freedom, since it describes a symmetry of the system. The magnitude of the complex field only becomes slow near threshold; far away it is just one of the many fast degrees of freedom.

We wish to consider spatiotemporal chaos and topological defects in an equation that has been used both as an “amplitude equation” in the sense discussed above as well as a model equation to study generic features of spatially extended nonlinear dynamical systems. We are using the equation as a model equation for spatiotemporal chaos; its applicability to real physical systems is limited to the weakly nonlinear regime. The complex Ginzburg–Landau equation we consider is given by

$$\partial_t A = (\mu_1 + i\mu_2)A - (c_1 + ic_2)|A|^2 A + (b_{1x} + ib_{2x})\partial_x^2 A + (b_{1y} + ib_{2y})\partial_y^2 A \quad (1)$$

where A is a complex field in two dimensions (see for example [36]). By rescaling $A' = \sqrt{\frac{c_1}{\mu_1}} A e^{-i\mu_2 t}$, $t' = \mu_1 t$, $x' = \sqrt{\frac{\mu_1}{b_{1x}}} x$, $y' = \sqrt{\frac{\mu_1}{b_{1y}}} y$, $b_x = \frac{b_{2x}}{b_{1x}}$, $b_y = \frac{b_{2y}}{b_{1y}}$, and $c = \frac{c_2}{c_1}$, we obtain the following equation (dropping now the primes):

$$\partial_t A = A - (1 + ic)|A|^2 A + (1 + ib_x)\partial_x^2 A + (1 + ib_y)\partial_y^2 A. \quad (2)$$

This equation can have topological defect solutions where $A = 0$ (both $\text{Re}[A]$ and $\text{Im}[A]$ are zero) [20, 21, 22, 23, 37, 38, 39, 40, 41]. These defects can occur either in static arrangements or in dynamic ones. The dynamics states can have defects moving in a regular fashion (for example, all defects drifting in one direction) or they can exhibit defect turbulence, where defects are continuously nucleated and annihilated in pairs and are moving about in a chaotic, non-regular fashion. We wish to focus on the latter case, the Benjamin–Feir turbulent instability regime [25, 42, 43, 44], which occurs when $1 + b_x c < 0$. In this region of parameter space, all spatially periodic solutions of the complex Ginzburg–Landau equation

are unstable. For comparison with the ideas of generic scale invariance [31, 32, 33, 34, 35], we will focus on the anisotropic case $b_x \neq b_y$.

The topological defects come in two varieties. The type of defect depends on how the phase of A changes as we travel counterclockwise once around the defect. A defect with a phase jump of 2π has a topological charge of $+1$, while one with a jump of -2π has a topological charge of -1 . This is analogous to the right-handed and left-handed single-armed spirals in Belousov–Zhabotinskii reactions [45]. Let $\rho_+(\mathbf{r})$ equal the density of $+1$ defects and $\rho_-(\mathbf{r})$ equal the density of -1 defects. We can then define a “topological” order parameter, $\rho(\mathbf{r}) \equiv \rho_+(\mathbf{r}) - \rho_-(\mathbf{r})$, which is just the density of the defects weighted by their topological charge. This order parameter is conserved in a system with periodic boundary conditions: $\int_V \rho(\mathbf{r}) d\mathbf{r} = 0$, as defects can only be created or destroyed in $+/-$ pairs. We focus on the order parameter $\rho(\mathbf{r})$ as an effective coarse-grained field, which, for the purpose of testing the applicability of generic scale invariance, we conjecture can be described by some hydrodynamic equation of motion. Figure 1 is a snapshot of the simulated system, showing the two types of defects, and lines of $\text{Re}[A] = 0$ and $\text{Im}[A] = 0$.

Although the time evolution of ensembles of defects is very complicated, considerable progress has been made in the study of the dynamics of isolated or weakly interacting defects. Defects are isolated singularities in the phase equation (for the phase of A), but are smooth solutions of the full equations. It is an attractive idea to imagine a description in terms of coupled dynamics of phase and defect degrees of freedom. Progress on this idea has been made in the case of Rayleigh–Bénard convection [9, 46, 47] and the Kuramoto–Sivaskinsky equation [8]; for a review of the situation in the complex Ginzburg–Landau equation see [10, pages 920–922].

The complex Ginzburg–Landau equation has also been studied in one dimension, where it also exhibits spatiotemporal chaos. Much effort has been made in this case to apply ideas from low-dimensional chaos, such as Lyapunov exponents and dimension densities [6, 48, 49, 50, 51, 52]. It is not clear that such ideas will be applicable to spatiotemporal chaos in general, or to the two-dimensional complex Ginzburg–Landau equation with topological defects in particular. In one-dimension, an important question, still unsettled, is whether phase turbulence (turbulence without strong amplitude fluctuations) exists [52]. In contrast, even an apparent phase turbulence regime has not been seen in the two-dimensional complex Ginzburg–Landau equation. The two dimensions (one versus two-dimensional) may very well be fundamentally different. Numerical simulations can provide insight into the relationship between these regimes.

3 Numerical Methods

Equation (2) is a continuum equation. We wish to put it in a form that allows approximate solution on a computer, which requires a discretization scheme, an eigenfunction expansion scheme, or some combination of both. We use a technique that combines elements of both approaches; it is a spectral method (for a general review of this see [53, 54]). This is a special form of a more general technique known as the method of weighted residuals [55, 56].

Our original code was obtained from P. Coulet, L. Gil, and J. Lega (see references [20, 21, 22, 23, 57]), and is now used as the basis for simulations by several groups. The

original code was simply the solution to the differential equation. We have optimized the code, speeding it up by a factor of 3; furthermore, we have added sections for analysis of defects and Fourier space quantities.

To begin our discussion of the numerical solution algorithm, we rewrite equation (2) as

$$\partial_t A = A + B_x \partial_x^2 A + B_y \partial_y^2 A - C|A|^2 A \quad (3)$$

where $B_x = 1 + ib_x$, $B_y = 1 + ib_y$, and $C = 1 + ic$. Now, if we knew the exact solution, equation (3) would be satisfied everywhere in space. However, we can only use a finite number of basis functions or grid points in a numerical solution method, so the solution we obtain is necessarily approximate. In order to make this approximation systematic, we define the residual

$$R(\mathbf{x}, t) \equiv \partial_t A - A + C|A|^2 A - B_x \partial_x^2 A - B_y \partial_y^2 A \quad (4)$$

for the numerical solution. In order for our numerical solution to be an accurate approximation to the full solution, this residual needs to be small. There are a number techniques that accomplish this and also fall under the general name “method of weighted residuals” [55, 56].

To formulate the numerical solution, the field $A(\mathbf{x}, t)$ is expanded

$$A(\mathbf{x}, t) = \sum_{\alpha=1}^{N_B} A_\alpha(t) \phi_\alpha(\mathbf{x}) \quad (5)$$

where $\phi_\alpha(\mathbf{x})$ is some basis function. Then we demand that

$$\int R(\mathbf{x}, t) \psi_\beta(\mathbf{x}) d\mathbf{x} = 0, \quad \beta = 1, \dots, N_B \quad (6)$$

where $\psi_\beta(\mathbf{x})$ is our weighting function. A variety of numerical techniques follow this general procedure. For example, if the basis set $\{\phi_\alpha\}$ is the same as $\{\psi_\beta\}$ then the method is known as a Galerkin technique. The finite element method can also be written in this general form [55, 56].

We use the “Fourier collocation” method [53, 54]. Note that we are always using periodic boundary conditions. For other types of boundaries (such as $A = 0$ at the boundaries), we could use Fourier sine transforms and expand in a basis set of sine waves. Our approach is to use

$$\phi_\alpha(\mathbf{x}) = e^{i\mathbf{k}_\alpha \cdot \mathbf{x}} \quad (7)$$

where $\mathbf{k}_\alpha = (\frac{2\pi}{L_x} k_1, \frac{2\pi}{L_y} k_2) = (k_x, k_y)$ for $k_1 = 0, \dots, N_x - 1$ and $k_2 = 0, \dots, N_y - 1$. This is the “Fourier” part. For the “collocation”, the residual is forced to be zero at the lattice points by choosing a set of delta functions for the weight functions

$$\psi_\beta(\mathbf{x}) = \delta(\mathbf{x} - \mathbf{x}_\beta) = \delta(x - x_{j_1}) \delta(y - y_{j_2}) \quad (8)$$

where $x_{j_1} = j_1 \delta x = j_1 \frac{L_x}{N_x}$ and $y_{j_2} = j_2 \delta y = j_2 \frac{L_y}{N_y}$, with $j_1 = 0, \dots, N_x - 1$ and $j_2 = 0, \dots, N_y - 1$.

At this point we define our conventions for the Fourier transform. The forward transform is

$$h_{k_1 k_2} = \frac{1}{N_x N_y} \sum_{j_1=0}^{N_x-1} \sum_{j_2=0}^{N_y-1} g_{j_1 j_2} e^{-2\pi i \frac{j_1 k_1}{N_x}} e^{-2\pi i \frac{j_2 k_2}{N_y}} \quad (9)$$

and the inverse transform is

$$g_{j_1 j_2} = \sum_{k_1=0}^{N_x-1} \sum_{k_2=0}^{N_y-1} h_{k_1 k_2} e^{2\pi i \frac{j_1 k_1}{N_x}} e^{2\pi i \frac{j_2 k_2}{N_y}}. \quad (10)$$

We calculate the Fourier transforms in the algorithm using IBM's Engineering and Scientific Subroutine Library (ESSL) Fast Fourier Transform (FFT) [58].

We now want to substitute equations (7) and (8) into equation (6). We will show this for the term $\partial_x^2 A$. Start with

$$\int \partial_x^2 A(\mathbf{x}, t) d\mathbf{x} = - \sum_{k_1 k_2} A_{k_1 k_2}(t) \left(\frac{2\pi k_1}{L_x} \right)^2 e^{2\pi i \frac{k_1 x}{L_x}} e^{2\pi i \frac{k_2 y}{L_y}} \delta(x - j_1 \delta x) \delta(y - j_2 \delta y) dx dy. \quad (11)$$

Performing the integral and recalling the definitions of δx , δy , and k_x gives

$$\sum_{k_1 k_2} A_{k_1 k_2}(t) k_x^2 e^{2\pi i \frac{k_1 j_1}{N_x}} e^{2\pi i \frac{k_2 j_2}{N_y}}. \quad (12)$$

Doing similar integrals for the other terms in $R(\mathbf{x}, t)$ and then using the inverse Fourier transform on the expressions (which amounts to dropping the terms $e^{2\pi i \frac{k_1 j_1}{N_x}}$ and $e^{2\pi i \frac{k_2 j_2}{N_y}}$ as well as the summation) gives us the equation (we write k for $k_1 k_2$)

$$\partial_t A_k(t) = (1 - B_x k_x^2 - B_y k_y^2) A_k(t) + N_k(t) \quad (13)$$

where $N_k(t)$ is the Fourier transform of $-C|A|^2 A$ (the nonlinear part of equation (3)). We simplify this even further by defining

$$L_k \equiv (1 - B_x k_x^2 - B_y k_y^2) \quad (14)$$

to give

$$\partial_t A_k(t) = L_k A_k(t) + N_k(t). \quad (15)$$

Multiplying both sides of equation (15) by an integrating factor $e^{-L_k t}$ and simplifying gives

$$\partial_t \left[e^{-L_k t} A_k(t) \right] = e^{-L_k t} N_k(t). \quad (16)$$

We then integrate from t to $t + \delta t$ to obtain

$$e^{-L_k(t+\delta t)} A_k(t + \delta t) - e^{-L_k t} A_k(t) = \int_t^{t+\delta t} e^{-L_k t'} N_k(t') dt' \quad (17)$$

or

$$A_k(t + \delta t) = e^{L_k \delta t} A_k(t) + e^{L_k(t+\delta t)} \int_t^{t+\delta t} e^{-L_k t'} N_k(t') dt'. \quad (18)$$

Now, consider the integral in equation (18). We approximate it as follows:

$$\int_t^{t+\delta t} e^{-L_k t'} N_k(t') dt' \approx N_k(t + \delta t) \int_t^{t+\delta t} e^{-L_k t'} dt' = N_k(t + \delta t) \left[\frac{e^{-L_k t} - e^{-L_k(t+\delta t)}}{L_k} \right]. \quad (19)$$

Substituting this into equation (18) yields

$$A_k(t + \delta t) = e^{L_k \delta t} A_k(t) + \left[\frac{e^{L_k \delta t} - 1}{L_k} \right] N_k(t + \delta t). \quad (20)$$

Finally, we use the Adams–Bashforth second–order time step for $N_k(t + \delta t)$:

$$N_k(t + \delta t) = \frac{3}{2} N_k(t) - \frac{1}{2} N_k(t - \delta t). \quad (21)$$

This gives us the full time step equation

$$A_k(t + \delta t) = e^{L_k \delta t} A_k(t) + \left[\frac{e^{L_k \delta t} - 1}{L_k} \right] \left[\frac{3}{2} N_k(t) - \frac{1}{2} N_k(t - \delta t) \right]. \quad (22)$$

The solution algorithm for equation (22) then consists of the following steps.

1. Calculate $-C|A|^2 A$ in real $(j_1 j_2)$ space.
2. Transform the result of step 1 to Fourier $(k_1 k_2)$ space to obtain $N_k(t)$.
3. Perform the time step given by equation (22) to obtain $A_k(t + \delta t)$. Save this result to use in calculating $A_k(t + 2\delta t)$.
4. Invert $A_k(t + \delta t)$ to obtain $A(\mathbf{x}, t + \delta t)$.
5. Save $N_k(t)$ to use in the Adams–Bashforth part of equation (22) for calculating $A_k(t + 2\delta t)$.

Analysis of various k –space quantities can be performed between steps 3 and 4 in the algorithm. For the initial time step we use $N_k(-\delta t) = N_k(0)$. We also have started our systems with two different types of initial conditions. The results do not depend upon which we choose. One initial condition is to seed the system with two oppositely charged topological defects. The other is to begin with random initial conditions (for instance a uniform distribution between -0.1 and 0.1 for the field A). After starting, we have to wait for the system to “equilibrate” to a steady–state condition (meaning fluctuations about an average number of defects). This takes, for our typical parameters, on the order of 5,000 time steps with a step size of $\delta t = 0.02$. The steady–state condition is a statistically stationary state, where averages depend only on differences of space and time coordinates.

By using a parallel (distributed) FFT, larger systems can be studied [59]. In the parallel algorithm, we distribute the data for the system over strips (*i.e.* the data for $j_1 = \frac{N_x}{N_P}(n - 1)$, $\frac{N_x}{N_P}n$ and $j_2 = 1, N_y$ exists on processor n , where N_P is the total number of processors). The $\frac{N_x}{N_P}$ FFT’s for the y (j_2) direction are calculated locally on each processor. We then perform a global transpose of the data for A by using collective communication (all to all) message passing. Once we have done this, the FFT’s for the x (j_1) direction are calculated locally on each processor. Then we have the result in Fourier space. To invert the FFT, we just reverse the process.

3.1 Improving the Time Step

The result given for equation (21) represents a somewhat uncontrolled approximation that was made in the original code in order to minimize storage requirements. There is a more accurate time step (which takes somewhat more storage), which we explain in this section (see [60] for a description of this process).

We wish to find an approximation to the equation:

$$I \equiv e^{L_k(t+\delta t)} \int_t^{t+\delta t} e^{-L_k t'} N_k(t') dt' \equiv e^{L_k(t+\delta t)} \int_{t_{p-j}}^{t_{p+l}} e^{-L_k t'} N_k(t') dt' \quad (23)$$

where $t_p = p\delta t = t$, $t_{p-j} = t_p - j\delta t$, and $t_{p+l} = t_p + l\delta t$. We then approximate $N_k(t')$ using an interpolating polynomial

$$N_k(t') \approx \sum_{i=0}^q N_k(t_{p-i}) L_i(t'), \quad (24)$$

where

$$L_i(t') = \prod_{l=0, l \neq i}^q \frac{t' - t_{p-l}}{t_{p-i} - t_{p-l}} \quad (25)$$

is the interpolating polynomial. Substituting this into (23) gives

$$I = e^{L_k(t+\delta t)} \sum_{i=0}^q N_k(t_{p-i}) \int_{t_{p-j}}^{t_{p+l}} e^{-L_k t'} L_i(t') dt'. \quad (26)$$

For comparison with the standard Adams–Bashforth formula, we are interested in the case $j = 0$, $l = 1$, and $q = 1$. Other choices for j , l , and q give other time-stepping schemes (*e.g.* Crank–Nicholson is given by $j = 1$, $l = 0$, and $q = 1$). For our case the interpolating polynomials are

$$L_0(t') = \frac{t' - t_{p-1}}{t_p - t_{p-1}} = \frac{t' - t + \delta t}{\delta t} \quad (27)$$

and

$$L_1(t') = \frac{t' - t_p}{t_{p-1} - t_p} = \frac{t' - t}{-\delta t}. \quad (28)$$

Using these results we obtain:

$$\int_{t_p}^{t_{p+1}} e^{-L_k t'} L_0(t') dt' = \frac{e^{-L_k t}}{L_k} \left[e^{-L_k \delta t} \left(-2 - \frac{1}{L_k \delta t} \right) + \left(1 + \frac{1}{L_k \delta t} \right) \right] \quad (29)$$

and

$$\int_{t_p}^{t_{p+1}} e^{-L_k t'} L_1(t') dt' = -\frac{e^{-L_k t}}{L_k} \left[e^{-L_k \delta t} \left(-1 - \frac{1}{L_k \delta t} \right) + \frac{1}{L_k \delta t} \right]. \quad (30)$$

The full integral (23) becomes

$$\begin{aligned} I = & N_k(t) \left[\frac{1}{L_k} \left(-2 - \frac{1}{L_k \delta t} \right) + \frac{e^{L_k \delta t}}{L_k} \left(1 + \frac{1}{L_k \delta t} \right) \right] \\ & - N_k(t - \delta t) \left[\frac{1}{L_k} \left(-1 - \frac{1}{L_k \delta t} \right) + \frac{e^{L_k \delta t}}{L_k^2 \delta t} \right]. \end{aligned} \quad (31)$$

In the limit $L_k \rightarrow 0$, equation (29) goes to $\frac{3}{2}\delta t$ and equation (30) goes to $-\frac{1}{2}\delta t$, which are just the results for the standard Adams–Bashforth second–order formula. Also, when L_k is held fixed and $\delta t \rightarrow 0$, the leading order terms become $\frac{3}{2}\delta t$ and $\frac{1}{2}\delta t$, with corrections of $O(\delta t^2)$, so that the original time step (equation (22)) is still “correct” to $O(\delta t)$. However, the improved time step developed in this section allows simulations to be run with a larger time increment δt for the same desired numerical accuracy. This time step method has been used for simulations of Rayleigh–Bénard convection [61]. Our results were obtained with the unimproved time step, but we present the improved version here so that others may take advantage of it.

4 Results for $A(\mathbf{x}, t)$

We present some results for the field $A(\mathbf{x}, t)$. First, Figure 2 shows that the field–field correlation function decays exponentially (or perhaps faster), and shows no hints of long–range order (such as a power law decay might suggest). We also note that the x and y directions show statistically different behavior. The y direction appears to show a domain type structure (as in, for example, spinodal decomposition [62]) for $r \approx 10$, because of the significant amount of negative correlations in that region. The x direction does not appear to show this behavior, as it decays smoothly to zero from its value at $r = 0$.

The exponential decay of the A – A correlation function has been observed in previous simulations [20, 21], and it was suggested by these authors that the defects are responsible for the strong decorrelation of the field. We can merely note here that the field $A(\mathbf{x}, t)$ is not conserved in time. This lack of a conservation law would imply, within the framework of generic scale invariance discussed below in Section 5, that the field–field correlation function should decay exponentially.

In Figure 3 we show the averaged power spectrum $\langle S(k_x) \rangle = \text{Re}\langle A^*(k_x)A(0) \rangle$; results are similar for $\langle S(k_y) \rangle$. This falloff is exponential (or perhaps faster), which is to be expected because of the fast decay of the field–field correlation function presented in Figure 2. The fact that the power spectrum decays rapidly to zero means that we don’t have problems with aliasing of the Fourier transform in the numerical method.

The probability of a particular value of $\text{Re}[A(x)]$ versus $\text{Re}[A(x)]$ is shown in Figure 4. This figure includes both spatial averaging at a particular time, as well as time averaging at a particular point in order to test the system’s ergodicity. The plot shows no special structure, and is not expected to, because principles that might give a special form, such as the Central Limit Theorem, do not apply to the measured quantity. Similar results are obtained for the probability of $\text{Im}[A(x)]$. We note that the two methods of averaging agree fairly well. We would expect that for larger systems and longer times the two results should agree. In Figure 5 we present the probability of a particular value of $|A(x)|$ versus $|A(x)|$, again with both types of averaging. Values of $|A|$ greater than 1.0 represent shock waves in the system, and the probability of larger and larger values of $|A|$ should decrease above $|A| = 1.0$. When $|A| = 0$, there is a defect in the system. This is expected to be rarer than other nonzero values, because it requires both $\text{Re}A = 0$ and $\text{Im}A = 0$. Both of these expected results are seen in the data.

In Figure 6 we show the result for the probability of $A(k)$ versus $A(k)$. Non–Gaussian

fluctuations in Fourier variables have been measured in capillary wave fields, and this has been used to question the applicability of a thermodynamic description for spatiotemporal chaos [63]. In contrast to the results for $A(x)$, we expect the Central Limit Theorem to hold for $A(k)$. This would then predict that the probability distribution function would be a Gaussian. In Figure 6 we compare our results to a Gaussian, and we see that we certainly have Gaussian fluctuations. Similar results hold for other wavevectors k for which we have measured this quantity. We also measured this probability distribution for these fluctuations for a different set of parameters ($c = -0.5$, $b_x = b_y = 40.0$) and started with a small system. The small system showed non-Gaussian fluctuations. When we went to larger systems, the fluctuations became Gaussian. This just means that for the small system there were not enough underlying degrees of freedom for the central limit theorem to be valid when we averaged in the system. Note that this small system also showed quasiperiodic behavior in the time series of $A(\mathbf{x}, t)$ for fixed \mathbf{x} . This system had $L_x = L_y = 60$. When we increased the size of the system to $L_x = L_y = 120$, this quasiperiodic behavior disappeared and was replaced by the chaotic behavior seen in [24]. This larger system was the one that also showed the Gaussian fluctuations.

Time averages of spatiotemporal chaos in experimental systems result in periodic spatial structures [64, 65]. We also tried averaging our amplitude $A(\mathbf{x}, t)$ over various times, and we did not see any particular persistent structures emerging. These results were not, however, from extensive tests. It is likely that the experimental results are due to the fixed boundary in these systems, which constrains the system to fluctuate about certain well-defined normal modes.

All of the above results for the field itself were not encouraging from the standpoint of illuminating special features of spatiotemporal chaos. We wish to examine another possible approach for describing the system, namely, generic scale invariance.

5 Generic Scale Invariance

In equilibrium systems, spatial correlations typically decay exponentially. For nonequilibrium systems, such as those with an external driving force, the situation can be quite different. For a nonequilibrium system with a conservation law and external noise, spatial correlation functions can decay algebraically. It has been suggested that this algebraic decay is expected to occur for a broad range of conditions, and this has been called “generic scale invariance” [31, 32, 33, 34, 35]. Some extended deterministic chaotic systems also exhibit algebraic decay [66, 67, 68]. In at least one of these examples, the chaotic fluctuations appear to play the same role as stochastic noise [66]. The complex Ginzburg–Landau equation would seem to satisfy the criterion for generic scale invariance; it shows nonequilibrium behavior since it cannot be derived from an underlying potential (*i.e.* it is non-relaxational), and in a system with periodic boundary conditions, the topological order parameter $\rho(\mathbf{r})$ is conserved. Finally, we conjecture that the chaotic noise in our system plays the role of stochastic noise, again for the purpose of testing the applicability of generic scale invariance.

With this set of conditions, we could have a hydrodynamic equation for the conserved order parameter (coarse grained over distances larger than the typical spacing between

defects):

$$\partial_t \rho(\mathbf{r}, t) = \Gamma\{\rho(\mathbf{r}, t)\} + \eta(\mathbf{r}, t) \quad (32)$$

where Γ is a general conserving operator on ρ , such as $\Gamma_0 \nabla^2 + \Gamma_1 (\nabla^2)^2 + \Gamma_{2x} \partial_x^4 + \Gamma_{2y} \partial_y^4$. It can also contain nonlinear terms (*e. g.* $\nabla \cdot [(\nabla^2 \rho)(\nabla \rho)]$). The stochastic noise term η is determined by:

$$\langle \eta(\mathbf{r}, t) \rangle = 0 \quad (33)$$

$$\langle \eta(\mathbf{r}, t) \eta(\mathbf{r}', t') \rangle = D \delta(\mathbf{r} - \mathbf{r}') \delta(t - t'), \quad (34)$$

where D must be composed of differential operators for our strictly conserved order parameter. This conserving noise term represents the effect of the chaotic fluctuations in the complex Ginzburg–Landau equation. There is evidence from the mapping of the Kuramoto–Sivashinsky equation to the Kardar–Parisi–Zhang equation [69, 70, 71] and from coupled map lattices [66] that this identification of spatiotemporal chaotic fluctuations with stochastic noise is not unreasonable. Note also that we are assuming that we can write down a local equation of motion for the order parameter ρ .

For systems with nonconserving noise (*i. e.* D is a constant), equation (32) is expected to always give rise to power law decays in the two point correlation function $G_\rho(\mathbf{r}) \equiv \langle \rho(\mathbf{r}) \rho(\mathbf{0}) \rangle$, as well as in higher order correlation functions. For nonlinear systems with conserving noise (*e. g.* $D = D_1 \nabla^2$) the situation is somewhat more complicated [32]. If the system is isotropic, then one obtains exponential decays in $G_\rho(\mathbf{r})$, but power law decays occur in higher order correlation functions. Systems which break isotropy give rise to algebraic decay in $G_\rho(\mathbf{r})$. For systems with cubic symmetry, one expects $G_\rho(\mathbf{r}) \sim 1/r^{d+2}$ for large r . For systems which break cubic symmetry one expects $G_\rho(\mathbf{r}) \sim 1/r^d$. We will study the last regime, a two–dimensional system with broken square symmetry, where generic scale invariance predicts that

$$G_\rho^{generic}(\mathbf{r}) = \langle \rho(\mathbf{r}) \rho(\mathbf{0}) \rangle \sim 1/r^2 \quad (35)$$

for large r [32]. We shall compare this prediction to the results from our numerics.

The ideas behind generic scale invariance depend upon showing that nonlinearities in the equations are irrelevant in a renormalization group sense. This means that as the scale on which the system is examined grows, the importance of the nonlinearities in the dynamics at the larger scale is less important. This analysis is usually carried out in a perturbative manner, where the strength of the nonlinear term is the small expansion parameter. It has proven notoriously difficult to treat topological defects in a perturbative manner. An example of this is the Kosterlitz–Thouless transition [72].

We also note that generic scale invariance requires short–ranged interactions. There is some evidence that this occurs for the defects in the complex Ginzburg–Landau equation [73, 74], but collective effects might be important. Finally, the mapping of chaotic fluctuations to the stochastic noise could break down. In the next section, we will prove that the predictions of generic scale invariance cannot apply to topological defects, and therefore at least one of the requirements for it to be present is lacking in our system.

6 Topological Constraints

We define the excess order parameter in a region to be

$$\delta\rho_L \equiv \left| \int_{\mathbf{r} \in B(L)} (\rho(\mathbf{r} + \mathbf{r}_0) - \rho_0) d\mathbf{r} \right|, \quad (36)$$

where $B(L)$ represents a circle of radius L about a point \mathbf{r}_0 , which we take as $\mathbf{r}_0 = \mathbf{0}$ due to translational invariance, and where ρ_0 is the average order parameter (in our case 0). For nontopological objects, the constraint is given by $\delta\rho_L \leq a_1 L^2$, where a_1 is some numerical constant. The excess of a nontopological object in a particular region must scale as the area of that region, since each individual object occupies a fixed area. For topological objects of the type we are studying, this constraint is different, *i. e.* $\delta\rho_L \leq a_2 L$, where a_2 is again some numerical constant. The constraint arises from the fact that any excess of topological defects in a region must be detectable simply by traversing the perimeter of that region. Each topological defect has an “arm” with characteristic width that must pass through the perimeter of the region. Examples of this are the spiral arms of the defects in Rayleigh–Bénard convection, extra rows of atoms for dislocations in crystals, and in our case lines of $\text{Re}[A] = 0$ and $\text{Im}[A] = 0$. When a region contains the maximum excess number of defects allowed, each of these lines takes up a fixed amount of the perimeter of the region. Since the maximum excess number of topological objects scales linearly with the number of lines, and the number of lines scales as the perimeter of the region, we must have that the maximum excess number of topological objects scales as the linear size L of the region.

If we assume that the correlation function $G_\rho(\mathbf{r})$ decays at the same asymptotic rate independent of the direction of \mathbf{r} , *i. e.* $G_\rho(\mathbf{r}) \sim f(\theta)g(r)$ where $g(r) \sim 1/r^\alpha$ for large r , then with this constraint we can show for two dimensions that α must be greater than 2, which contradicts the prediction of generic scale invariance. This result also requires that $\int_0^{2\pi} f(\theta)d\theta \neq 0$, which we expect to be true except for special cases; we discuss this point further in Section 6.1 below. A correlation function satisfying both assumptions occurs, for example, in studies of non-equilibrium conservative anisotropic lattice gases [75, 76]. To show that $\alpha > 2$, we use the inequality $\delta\rho_L \leq aL$. Squaring this relation yields

$$\int_{\mathbf{r} \in B(L)} \int_{\mathbf{r}' \in B(L)} d\mathbf{r} d\mathbf{r}' \rho(\mathbf{r}, t) \rho(\mathbf{r}', t) \leq a^2 L^2. \quad (37)$$

Now we average over the noise (or over space and time, depending upon how you wish to look at it)

$$\langle \rho(\mathbf{r}, t) \rho(\mathbf{r}', t) \rangle \rightarrow G_\rho(\mathbf{r} - \mathbf{r}'). \quad (38)$$

This then gives the constraint equation

$$\langle \delta\rho_L^2 \rangle \leq a^2 L^2 \quad (39)$$

We now make the assumption that we can write $G_\rho(\mathbf{r})$ in the form $f(\theta)g(r)$ where θ is the angle for \mathbf{r} and $r = |\mathbf{r}|$. Strictly speaking, this assumption is only necessary for large r . Given that G_ρ takes this form, we can write

$$\int_{\mathbf{r} \in B(L)} \int_{\mathbf{r}' \in B(L)} d\mathbf{r} d\mathbf{r}' G_\rho(\mathbf{r} - \mathbf{r}') = \frac{1}{2\pi} \int_0^{2\pi} f(\theta) d\theta \int_0^{2L} g(R) w(R) dR, \quad (40)$$

where $w(R)$ is given by

$$w(R) = \int_{\mathbf{r} \in B(L)} \int_{\mathbf{r}' \in B(L)} S(R) \delta(\mathbf{r} - \mathbf{r}' - \mathbf{R}) d\mathbf{r} d\mathbf{r}' \quad (41)$$

with $S(R) = 2\pi R$ the surface area of the circle of radius R . We further will assume that $\int_0^{2\pi} f(\theta) d\theta \neq 0$, and now calculate a closed form expression for $w(R)$. To do this we use the definition of $\delta(\mathbf{x})$:

$$\delta(\mathbf{x}) \equiv \frac{1}{(2\pi)^2} \int_{-\infty}^{\infty} d\mathbf{k} e^{i\mathbf{k} \cdot \mathbf{x}}. \quad (42)$$

Plugging this into equation (41) gives

$$w(R) = \frac{2\pi R}{(2\pi)^2} \int_{-\infty}^{\infty} d\mathbf{k} e^{-i\mathbf{k} \cdot \mathbf{R}} \int_{\mathbf{r} \in B(L)} d\mathbf{r} e^{i\mathbf{k} \cdot \mathbf{r}} \int_{\mathbf{r}' \in B(L)} d\mathbf{r}' e^{-i\mathbf{k} \cdot \mathbf{r}'}. \quad (43)$$

The integrals over $B(L)$ are given by

$$\int_{\mathbf{r} \in B(L)} d\mathbf{r} e^{i\mathbf{k} \cdot \mathbf{r}} = \int_0^L \int_0^{2\pi} r dr d\theta e^{ikr \cos \theta} = \frac{2\pi L}{k} J_1(kL), \quad (44)$$

where J_1 is the first order Bessel function. Substituting this result in equation (43), we obtain

$$w(R) = 2\pi RL^2 \int_{-\infty}^{\infty} d\mathbf{k} e^{-i\mathbf{k} \cdot \mathbf{R}} \frac{J_1^2(kL)}{k^2} = 4\pi^2 RL^2 \int_0^{\infty} \frac{dk}{k} J_0\left(k\frac{R}{L}\right) J_1^2(k). \quad (45)$$

Performing this last integral [77] gives

$$w(R) = 4\pi RL^2 \left[\cos^{-1}\left(\frac{R}{2L}\right) - \frac{R}{2L} \sqrt{1 - \left(\frac{R}{2L}\right)^2} \right]. \quad (46)$$

We can check this by noting that $\int_0^{2L} w(R) dR = \pi^2 L^4$, which is just $\left(\int_{\mathbf{r} \in B(L)} d\mathbf{r}\right)^2$.

Next, we apply $w(R)$ to the problem at hand. Suppose that $g(R)$ in equation (40) exhibits its asymptotic behavior outside of some $R = r_{min}$, $g(R) \sim R^{-\alpha}$ for $R > r_{min}$ and also that $L \gg r_{min}$. Splitting the integral into two parts yields

$$\int_0^{2L} g(R) w(R) dR = \int_{r_{min}}^{2L} + \int_0^{r_{min}} g(R) w(R) dR. \quad (47)$$

We consider each of these terms separately. The second term can be bounded in the following manner:

$$\left| \int_0^{r_{min}} g(R) w(R) dR \right| \leq |g_{max}| \int_0^{r_{min}} w(R) dR. \quad (48)$$

Expanding the integral of $w(R)$ in descending powers of L gives

$$\left| \int_0^{r_{min}} g(R) w(R) dR \right| \leq \pi^2 r_{min}^2 g_{max} L^2 + O(L). \quad (49)$$

We calculate the first integral in equation (47) next. Assuming that $g(R) = g_0 R^{-\alpha}$, we substitute equation (46) for $w(R)$ and write the integral as

$$4\pi L^2 (2L)^{2-\alpha} g_0 \int_{\frac{r_{min}}{2L}}^1 \left[\eta^{1-\alpha} \cos^{-1} \eta - \eta^{2-\alpha} (1 - \eta^2)^{\frac{1}{2}} \right] d\eta. \quad (50)$$

We again expand this integral in descending powers of L . There are no singularities due to the upper limit of 1, since the integrand is analytic there for all α . However, at the lower limit, as $L \rightarrow \infty$, there can be divergences, depending on the value of α . The integrand, upon expansion about $\eta = 0$, becomes

$$\eta^{-\alpha} \left[\frac{\pi}{2} \eta - 2\eta^2 + O(\eta^4) \right]. \quad (51)$$

Now, suppose that $\alpha < 2$. Then the integrand has an integrable singularity at $\eta = 0$, and as $L \rightarrow \infty$ we obtain some constant plus correction terms that die away for large L . For $\alpha = 2$ we get a logarithmic divergence, and for $\alpha > 2$ a diverging term $L^{\alpha-2}$ which exactly cancels the $L^{2-\alpha}$ in front of equation (50).

The leading order behavior of $\langle \delta\rho_L^2 \rangle$ is then

$$\begin{aligned} \alpha < 2 & : \langle \delta\rho_L^2 \rangle \sim L^2 L^{2-\alpha} \\ \alpha = 2 & : \langle \delta\rho_L^2 \rangle \sim L^2 \log(L) \\ \alpha > 2 & : \langle \delta\rho_L^2 \rangle \sim L^2. \end{aligned} \quad (52)$$

Recall that the result for generic scale invariance is the case $\alpha = 2$ (see equation (35)). However, this case violates the constraint given by equation (39). Within our assumptions, this result means that for topological objects the results of generic scale invariance cannot hold. In fact, what we have provided is a bound on α . For topological objects, α must be strictly greater than 2. Generic scale invariance predicts $\alpha = 2$. The simple geometric nature of topological objects prevents them from having correlation functions that decay as certain power laws. (A decay of $1/(r^2(\log r)^\beta)$ for $\beta > 1$ satisfies our bounds on $\langle \delta\rho_L^2 \rangle$, but contradicts the predictions of generic scale invariance.) An added conclusion from the consideration of the topological constraints is that if the topological objects form ordered states, they must be of the antiferromagnetic variety (*e.g.* alternating + and - vortices) in at least one direction, in order to satisfy the topological constraint. An example of such a state in the complex Ginzburg–Landau equation has been seen, with defects ordering along chains where the defects in one chain are of opposite sign from the defects in neighboring chains [78].

In our analysis we have only considered the largest possible fluctuations. We expect these fluctuations to be rare, and hence expect a faster decay than the bound we provide. As an analogy, for nontopological objects the analysis presented here would predict that the correlation function can be at most a constant for large r ; in practice, systems like spins or atoms have connected correlation functions that decay to zero, either as power laws or as exponentials. However, it is often true that inequalities in physics are saturated, especially in relationships between critical exponents for phase transitions. This could be the case here, but numerically it appears that we do not saturate this bound, as will be shown in Section 7 below.

6.1 Splitting the Correlation Function

One further point that we should consider is the splitting of the correlation function into angular and radial components. We mentioned above that this is important for our analysis. We cannot explicitly show this for the topological defects, but we can demonstrate this splitting in the context of generic scale invariance. Starting with the general result for the correlation function

$$G(\mathbf{r}) = \int d\mathbf{k} e^{i\mathbf{k}\cdot\mathbf{x}} \frac{D(\mathbf{k})}{\Gamma(\mathbf{k})} \quad (53)$$

we then define

$$G(r) = \frac{1}{2\pi} \int_0^{2\pi} G(\mathbf{r}) d\theta \quad (54)$$

where $\mathbf{r} = (r \cos \theta, r \sin \theta)$. Then

$$G(r) = \frac{1}{2\pi} \int_0^{2\pi} d\theta \int d\mathbf{k} \frac{D(\mathbf{k})}{\Gamma(\mathbf{k})} e^{i(k_x r \cos \theta + k_y r \sin \theta)}. \quad (55)$$

Performing the θ integral yields

$$G(r) = \int d\mathbf{k} \frac{D(\mathbf{k})}{\Gamma(\mathbf{k})} J_0(r \sqrt{k_x^2 + k_y^2}), \quad (56)$$

where J_0 is the zeroth order Bessel function. Note that this expression is not in general zero.

We can give a concrete expression, in a particular limit, for $G(r)$. We begin with specific expressions for $D(\mathbf{k})$ and $\Gamma(\mathbf{k})$, and ignore questions of convergence of the integrals for large k . Consider

$$G(\mathbf{r}) = \int_{-\infty}^{\infty} \int_{-\infty}^{\infty} dk_x dk_y e^{i(k_x x + k_y y)} \left(\frac{ak_x^2 + bk_y^2}{ck_x^2 + dk_y^2} \right). \quad (57)$$

The k_x integral can be performed as a contour integral; the expression has poles at $k_x = \pm i\sqrt{d/ck_y} \equiv \pm i\gamma k_y$. We assume for ease of calculation the $x > 0$ and $y > 0$; the results are the same for other cases. When $k_y > 0$, we close the contour in the upper half of the complex k_x plane, enclosing the pole at $i\gamma k_y$. For $k_y < 0$ we enclose the pole at $-i\gamma k_y$. The integral then becomes $2\pi i$ times the residue at $k_x = i\gamma k_y$. Then we obtain

$$G(\mathbf{r}) = \frac{\pi}{c\gamma} (b - a\gamma^2) \left(\int_0^{\infty} dk_y k_y e^{-k_y(\gamma x - iy)} + \int_{-\infty}^0 dk_y k_y e^{-k_y(-\gamma x - iy)} \right). \quad (58)$$

By performing the k_y integrals we obtain (using $x = r \cos \theta$ and $y = r \sin \theta$)

$$G(\mathbf{r}) = \frac{2\pi(bc - ad)}{\sqrt{cd}} \left(\frac{d \cos^2 \theta - c \sin^2 \theta}{(d \cos^2 \theta + c \sin^2 \theta)^2} \right) \frac{1}{r^2} \quad (59)$$

Note that our results are for the case $c \neq d$, so we have for this simple example the result that the angular average is not zero. Also, equation (59) is explicitly split into a radial and angular component.

7 Numerical Results for the Defects

We have numerically solved equation (2) with periodic boundary conditions in the turbulent regime using a Fourier collocation code. We choose $L_x = 240$, $L_y = 240$, $N_x = 360$, and $N_y = 360$ (see Section 3 above). We use the parameter values $c = 1.5$, $b_x = -0.75$, and $b_y = -3.0$. The time step used was $\delta t = 0.02$. We initially “equilibrate” from a state with two oppositely charged defects to a state with fluctuations about some average number of defects. This typically takes 5000 time steps. We note that the defects do not form bound pairs. When a pair is created, the defects tend to move apart, and when they eventually annihilate, they usually do so with a defect other than their initial partner. This illustrates that the system is not in a Kosterlitz–Thouless bound pair phase [72]. Figure 1 shows a snapshot of part of our system.

Topological defects have been studied in systems undergoing phase ordering. In these systems (an example is the XY model) the existence of an underlying Hamiltonian allows analytic progress to be made [79, 80] in the form of perturbation expansions. Some numerical work has also been performed on these systems [81]. For our system, the numerical results are key as we cannot form perturbation expansions due to the lack of an underlying Hamiltonian. These numerical calculations must begin with the determination of the location of the defects.

To find the defects in our system, we examine the change in the phase of A as each plaquette (or square unit cell) on our lattice in real space is traversed counterclockwise. To do this, we examine the phase $\varphi(\mathbf{x}, t) \equiv \tan^{-1} \left(\frac{\text{Im } A(\mathbf{x}, t)}{\text{Re } A(\mathbf{x}, t)} \right)$ as we go around a plaquette on the lattice and sum up the phase differences between the four points in the plaquette. A change of 0 signifies that the plaquette does not contain a defect, while changes of $\pm 2\pi$ reveal that a defect exists in the plaquette. We can actually speed up the defect finding process a bit. If all four sites in the plaquette have the same sign of $\text{Re } [A]$ or of $\text{Im } [A]$, then the plaquette cannot contain a defect. More complicated situations can also be handled, such as where one corner of the plaquette is of a different sign from the other three corners for $\text{Re } [A]$, while the opposite corner from the original one is of a different sign from the other three corners for $\text{Im } [A]$. In this case, the plaquette cannot contain a defect. These considerations avoid the costly calculation of \tan^{-1} , and can be used for a large fraction of the plaquettes in the lattice.

Once we have found the defects, we can calculate $n(t)$, the total number of defects in the system, and $G_\rho(\mathbf{r})$. To do the averaging, we have run for 750,000 time steps. We only sample $G_\rho(\mathbf{r})$ and $n(t)$ every 10 time steps, because adjacent time steps are not statistically independent. We have calculated that $\langle n(t)n(0) \rangle - \langle n \rangle^2 \sim e^{-t/\tau}$, with $\tau \sim 115$ time steps. It has been predicted [22] that the probability of finding a particular value of n in the system is given by $P(n) \sim e^{-(n-\langle n \rangle)^2/2\langle n \rangle}$. We have calculated the various moments of our distribution $P(n)$, and we find $\langle n \rangle = 422.8 \pm 0.3$, $\sigma^2 = 397 \pm 30$, as well as a skewness of 0.014 and a kurtosis of -0.026 , which is in good agreement with the predictions from reference [22]. In Figure 7, we present a plot of the results for $P(n)$ together with the fitted exponential. The agreement is quite remarkable.

In Figure 8 we present the results for $G_\rho(\mathbf{r})$ with \mathbf{r} in both the \hat{x} and \hat{y} directions. For both directions the typical nearest neighbor is of the opposite sign: the charges are thus screened. Similar behavior for vortices in random wave fields has been observed [82]. In

Figure 9 we show a linear–log plot of $|G_\rho(r)|$. In Figure 10 we show log–log plots of $|G_\rho(r)|$. We also show lines that represent the slope $|G_\rho(r)|$ should have if it decayed like $1/r^2$. We note that at the right edge of the figure, we have reached the point where our data is dominated by statistical noise. It is clear that neither direction shows the expected $1/r^2$ decay. Our results are at variance with the predictions of generic scale invariance, as they must be. As was shown in the last section, the theory is not applicable to systems which have strong constraints placed on them due to the topological nature of the order parameter.

The suggestion has been made [83] that in order to see the $1/r^2$ decay the system needs to break $x \rightarrow -x$ symmetry. We systematically tested this idea by adding various terms to the original equation (2).

First, we added a term $d\partial_x A$ to the equation. This term does break the $x \rightarrow -x$ symmetry. The result for the correlation function $G_\rho(r)$ is given in Figure 11. The results are similar to the ones seen in Figure 10 for the results of the original equation. Note that the term we have added here actually only induces a drift in the entire pattern, and can be scaled away, so it is not surprising that it does not show behavior that differs from the original equation.

Second, we added the term $d\partial_x^3 A$ to the original equation. The result for $G_\rho(r)$ is shown in Figure 12. This term also breaks the $x \rightarrow -x$ symmetry. However, a term of this form is expected to show, according to the ideas of generic scale invariance [83], a decay that is actually faster than $1/r^2$, so our results are not very informative. We cannot distinguish between power laws of $1/r^4$ and our results, so we must proceed to add a different term to the original equation.

The third new term we added both breaks the $x \rightarrow -x$ symmetry and *is* expected to show a $1/r^2$ decay, according to the predictions of generic scale invariance. This term is $d\partial_x(|A|^2 A)$. The numerical results for $G_\rho(r)$ are shown in Figure 13. We see from this that the correlation function does not decay like $1/r^2$. This is not surprising in the light of our results from Section 6, which apply to any two–dimensional topological defect in a complex field.

Finally, we experimented with breaking the $A \rightarrow -A$ symmetry in the original equation by adding the term $d\partial_x A^2$ to the original equation. The results for $G_\rho(r)$ are given in Figure 14. These results no longer shows the strong anisotropy seen in the correlation function of the original unmodified equation. With the broken symmetry, the decay of the correlation function in the \hat{y} direction occurs smoothly to zero from the negative values near $r = 0$ without crossing zero.

We have also constructed a coarse–grained order parameter field by defining

$$\rho_{cg}(\mathbf{r}) \equiv \int d\mathbf{s} h(\mathbf{s}) \rho(\mathbf{r} - \mathbf{s}) \quad (60)$$

where $h(\mathbf{s})$ is a coarse–graining weight function with $\int d\mathbf{s} h(\mathbf{s}) = 1$. We will use the Gaussian $h(\mathbf{s}) = \frac{1}{2\pi\sigma^2} e^{-s^2/2\sigma^2}$. With this we can also calculate $G_{\rho_{cg}}(r)$. The result is shown in Figure 15. We can examine the leading behavior of this correlation function by noting that

$$G_{\rho_{cg}}(\mathbf{r}) = \langle \rho_{cg}(\mathbf{r}) \rho_{cg}(\mathbf{0}) \rangle = \int \int d\mathbf{s} d\mathbf{s}' h(\mathbf{s}) h(\mathbf{s}') \langle \rho(\mathbf{r} - \mathbf{s}) \rho(-\mathbf{s}') \rangle. \quad (61)$$

This can be rewritten as

$$G_{\rho_{cg}}(\mathbf{r}) = \int \int ds ds' \frac{1}{(2\pi\sigma^2)^2} e^{-\frac{1}{2\sigma^2}(s^2+s'^2)} G_\rho(\mathbf{r} - (\mathbf{s} - \mathbf{s}')). \quad (62)$$

We now change variables $\boldsymbol{\xi} \equiv \mathbf{s} - \mathbf{s}'$ and $\boldsymbol{\eta} \equiv \mathbf{s} + \mathbf{s}'$ to obtain

$$G_{\rho_{cg}}(\mathbf{r}) = \frac{1}{(2\pi\sigma^2)^2} \int \int d\boldsymbol{\xi} d\boldsymbol{\eta} e^{-\eta^2/4\sigma^2} e^{-\xi^2/4\sigma^2} G_\rho(\mathbf{r} - \boldsymbol{\xi}). \quad (63)$$

We can perform the η integral to obtain the final result:

$$G_{\rho_{cg}}(\mathbf{r}) = \frac{1}{\pi\sigma^2} \int d\boldsymbol{\xi} e^{-\xi^2/4\sigma^2} G_\rho(\mathbf{r} - \boldsymbol{\xi}). \quad (64)$$

Using this final equation, we can explain the Gaussian decay seen in Figure 15. Typically, the microscopic field $G_\rho(\mathbf{r})$ will be given by $G_0\delta(\mathbf{r}) + g(\mathbf{r})$. Plugging this into equation (64) gives

$$G_{\rho_{cg}}(\mathbf{r}) = \frac{G_0}{\pi\sigma^2} e^{-r^2/4\sigma^2} + \frac{1}{\pi\sigma^2} \int d\boldsymbol{\xi} e^{-\xi^2/4\sigma^2} g(\mathbf{r} - \boldsymbol{\xi}). \quad (65)$$

The behavior of the correlation function in Figure 15 for small r is approximately Gaussian, due to the leading term in equation (65) as well as corrections to the overall decay due to the second term in equation (65). For larger r we see the domain structure of the coarse grained field ρ_{cg} . We do not see any evidence of power-law decays in this coarse-grained correlation function.

As a final comment on the numerical results presented in this section, note that the typical spacing between defects in our parameter regime is fairly large. As a result, we are not able to obtain adequate statistics for the correlation functions for large r , and we might not have reached the asymptotic regime where generic scale invariance should apply. Also, the results for the noisier (\hat{y}) direction do not convincingly rule out $1/r^2$ behavior. However, the proof we have provided in Section 6 shows analytically that the topological nature of the defects precludes $1/r^2$ decay in the correlation function.

8 Conclusions

We have calculated a number of quantities of interest in the complex Ginzburg–Landau equation. These have included both properties that depend on the amplitude field A and properties that depend upon the defect order parameter ρ . The results for the field A provide information about the reliability of our numerics, as well as suggesting that the Central Limit Theorem holds for k -space quantities.

The results for the order parameter field ρ did not agree with the predictions of generic scale invariance [31, 32, 33]. This places a limit on the applicability of generic scale invariance. Conversely, the results also place a bound on the types of coarse-grained, statistical theories that can be used to describe spatiotemporally chaotic systems with topological defects.

9 Acknowledgments

We would like to thank P. C. Hohenberg, J. F. Marko, and M. E. J. Newman for helpful conversations. This work was partly funded by the Hertz Foundation (BWR), the NSF under grant DMR-91-18065 (BWR, JPS), and the Alfred P. Sloan Foundation (EB). We also thank the Cornell Materials Science Center for the use of its computational resources.

References

- [1] E. Ott, *Chaos in Dynamical Systems* (Cambridge University Press, New York, 1993).
- [2] M. C. Cross and P. C. Hohenberg, *Science* 263 (1994) 1569.
- [3] K. Kaneko, ed., *Theory and Applications of Coupled Map Lattices* (Wiley, New York, 1993).
- [4] S. Ciliberto and M. Caponeri, *Phys. Rev. Lett.* 64 (1990) 2775.
- [5] J. Miller and D. A. Huse, *Phys. Rev. E* 48 (1993) 2528.
- [6] P. C. Hohenberg and B. I. Shraiman, *Physica D* 37 (1989) 109.
- [7] M. S. Bourzutschky and M. C. Cross, *Chaos* 2 (1992) 173.
- [8] C. C. Chow and T. Hwa, preprint cond-mat #9412041 (1994).
- [9] M. C. Cross and Y. Tu, preprint (1994).
- [10] M. C. Cross and P. C. Hohenberg, *Rev. Mod. Phys.* 65 (1993) 851.
- [11] E. Bodenschatz, J. DeBruyn, G. Ahlers, and D. Cannell, *Phys. Rev. Lett.* 67 (1991) 3078.
- [12] S. W. Morris, E. Bodenschatz, D. S. Cannell, and G. Ahlers, *Phys. Rev. Lett.* 71 (1993) 2026.
- [13] S. W. Morris, E. Bodenschatz, and J. R. de Bruyn, *Physics in Canada* 50 (1994) 9.
- [14] M. Assenheimer and V. Steinberg, *Nature* 367 (1994) 345.
- [15] S. Kai and K. Hirakawa, *Suppl. Prog. Theor. Phys.* 64 (1978) 212.
- [16] I. Rehberg, S. Rasenat, and V. Steinberg, *Phys. Rev. Lett.* 62 (1989) 756.
- [17] E. Braun, S. Rasenat, and V. Steinberg, *Europhysics Lett.* 15 (1991) 597.
- [18] N. B. Tufillaro, R. Ramashankar, and J. P. Gollub, *Phys. Rev. Lett.* 62 (1989) 422.
- [19] A. C. Newell and J. V. Moloney, *Nonlinear Optics* (Addison–Wesley, New York, 1992).
- [20] P. Couillet, L. Gil, and J. Lega, *Phys. Rev. Lett.* 62 (1989) 1619.
- [21] P. Couillet, L. Gil, and J. Lega, *Physica D* 37 (1989) 91.
- [22] L. Gil, J. Lega, J. L. Meunier, *Phys. Rev. A* 41 (1990) 1138.
- [23] J. Lega, *Comp. Meth. in Appl. Mech. and Eng.* 89 (1991) 419.
- [24] I. Aranson, L. Kramer, and A. Weber, *Phys. Rev. Lett.* 72 (1994) 2316.

- [25] A. C. Newell, in *Nonlinear Wave Motion*, edited by A. C. Newell, (American Mathematical Society, Providence, R. I., 1974).
- [26] S. Nasuno and S. Kai *Europhysics Lett.* 14 (1991) 779.
- [27] S.-I. Sasa, *Prog. Theor. Phys.* 83 (1990) 824.
- [28] J. M. Davidenko, A. V. Pertsov, R. Salomonsz, W. Baxter, and J. Jalife, *Nature* 355 (1993) 349.
- [29] Q. Ouyang and H. L. Swinney, *Chaos* 1 (1991) 411.
- [30] J. Lega, J. V. Moloney, and A. C. Newell, *Phys. Rev. Lett.* 73 (1994) 2978, and references therein.
- [31] G. Grinstein, D.-H. Lee, and S. Sachdev, *Phys. Rev. Lett.* 64 (1990) 1927.
- [32] G. Grinstein, *J. Appl. Phys.* 69 (1991) 5441.
- [33] G. Grinstein, C. Jayaprakash, and J. E. S. Socolar, *Phys. Rev. E* 48 (1993) 643.
- [34] G. Grinstein and D.-H. Lee *Phys. Rev. Lett.* 66 (1991) 177.
- [35] P. L. Garrido, J. L. Lebowitz, C. Maes, and H. Spohn, *Phys. Rev. A* 42 (1990) 1954.
- [36] L. Kramer, F. Hynne, P. Graae Sørensen, and D. Walgraef, *Chaos* 4 (1994) 443.
- [37] Y. Kuramoto, *Chemical Oscillations, Waves, and Turbulence* (Springer-Verlag, New York, 1984).
- [38] P. S. Hagan, *SIAM J. Appl. Math.* 42 (1982) 762.
- [39] E. Bodenschatz, A. Weber, and L. Kramer, in *Nonlinear Wave Processes in Excitable Media*, A. Holden, M. Markus, and H. Othmer, eds. (Plenum Press, New York, 1991).
- [40] G. Huber, P. Alstrøm, and T. Bohr, *Phys. Rev. Lett.* 69 (1992) 2380.
- [41] H. Sakaguchi, *Prog. Theor. Phys.* 82 (1989) 7.
- [42] T. B. Benjamin and J. E. Feir, *J. of Fluid Mech.* 27 (1967) 417.
- [43] J. T. Stuart and R. C. DiPrima, *Proc. Roy. Soc. Lond. A* 362 (1978) 27.
- [44] R. Brown, A. L. Fabrikant, and M. I. Rabinovich, *Phys. Rev. E* 47 (1993) 4141.
- [45] S. C. Müller, T. Plesser, and B. Hess, *Physica D* 24 (1987) 71; *Physica D* 24 (1987) 87.
- [46] M. C. Cross and A. C. Newell, *Physica D* 10 (1984) 299.
- [47] A. C. Newell, T. Passot, and M. Souli, *Phys. Rev. Lett.* 64 (1990) 2378; *J. Fluid Mech.* 220 (1990) 187.

- [48] B. I. Shraiman et al., *Physica D* 57 (1992) 241.
- [49] H. Chaté, *Nonlinearity* 7 (1994) 185; and also in *Spatio-temporal Patterns in Nonequilibrium Complex Systems*, edited by P. E. Cladis and P. Palffy-Muhoray, (Addison-Wesley, New York, 1995).
in *Nonlinear Wave Motion*, edited by A. C. Newell, (American Mathematical Society, Providence, R. I., 1974).
- [50] D. A. Egolf and H. S. Greenside, *Nature* 369 (1994) 129.
- [51] T. Bohr, E. Bosch, and W. van de Water, *Nature* 372 (1994) 48.
- [52] D. A. Egolf and H. S. Greenside, *Phys. Rev. Lett.* 74 (1995) 1751.
- [53] C. Canuto, M. Y. Hussaini, A. Quarteroni, and T. A. Zang, *Spectral Methods in Fluid Dynamics* (Springer-Verlag, New York, 1988).
- [54] D. Gottlieb and S. A. Orszag, *Numerical Analysis of Spectral Methods: Theory and Applications* (SIAM, Philadelphia, 1977).
- [55] C. A. J. Fletcher, *Computational Galerkin Methods* (Springer-Verlag, New York, 1984).
- [56] C. A. J. Fletcher, *Computational Techniques for Fluid Dynamics, Volume I* (Springer-Verlag, New York, 1988).
- [57] P. Couillet, C. Elphick, L. Gil, and J. Lega, *Phys. Rev. Lett.* 59 (1987) 884.
- [58] *Engineering and Scientific Subroutine Library, Version 2: Guide and Reference* (IBM Corporation, Kingston, New York, 1992).
- [59] M. Meyer, B. Roberts, C. Myers, and E. Bodenschatz, unpublished (1995).
- [60] J. Stoer and R. Bulirsch, *Introduction to Numerical Analysis* (Springer-Verlag, New York, 1980).
- [61] W. Decker, W. Pesch, and A. Weber, *Phys. Rev. Lett.* 73 (1994) 648; W. Pesch, private communication.
- [62] See for example S. N. Majumdar, D. A. Huse, and B. D. Lubachevsky, *Phys. Rev. Lett.* 73 (1994) 182.
- [63] E. Bosch and W. van de Water, *Phys. Rev. Lett.* 70 (1993) 3420.
- [64] L. Ning, Y. Hu, R. E. Ecke, and G. Ahlers, *Phys. Rev. Lett.* 71 (1993) 2216.
- [65] B. J. Gluckman, P. Marcq, J. Bridger, and J. P. Gollub, *Phys. Rev. Lett.* 71 (1993) 2034.
- [66] R. Bhagavatula, G. Grinstein, Y. He, and C. Jayaprakash, *Phys. Rev. Lett.* 69 (1992) 3483.

- [67] D. Hansel and H. Sompolinsky, Phys. Rev. Lett. 71 (1993) 2710.
- [68] M. Eisele, Physica D 48 (1991) 295.
- [69] C. Jayaprakash, F. Hayot, and R. Pandit, Phys. Rev. Lett. 71 (1993) 12.
- [70] V. L'vov and I. Procaccia, Phys. Rev. Lett. 72 (1993) 307.
- [71] C. Jayaprakash, F. Hayot, and R. Pandit, Phys. Rev. Lett. 72 (1993) 308.
- [72] P. Minnhagen, Rev. Mod. Phys. 59 (1987) 1001.
- [73] I. S. Aranson, L. Kramer, and A. Weber, Phys. Rev. E 47 (1993) 3231.
- [74] I. S. Aranson, L. Kramer, and A. Weber, Physica D 53 (1991) 376.
- [75] Z. Cheng, P. L. Garrido, J. L. Lebowitz, and J. L. Vallés, Europhysics Lett. 14 (1991) 507.
- [76] M. Q. Zhang, J.-S. Wang, J. L. Lebowitz, and J. L. Vallés, J. Stat. Phys. 52 (1988) 1461.
- [77] A. P. Prudnikov, Yu. A. Brychkov, and O. I. Marichev, Integrals and Series (Gordon and Breach Science Publishers, New York, NY, 1986), volume 2, p. 232. Note that there is a mistake in the formula given. $\frac{1}{\pi}\cos^{-1}() - c\sqrt{}$ should be $\frac{1}{\pi}\left(\cos^{-1}() - c\sqrt{}\right)$.
- [78] A. Weber, E. Bodenschatz, and L. Kramer, Adv. Mat. 3 (1991) 191.
- [79] B. I. Halperin, in Physics of Defects, R. Balian *et al.*, eds. (North-Holland, New York, 1981).
- [80] F. Liu and G. F. Mazenko, Phys. Rev. B 46 (1992) 5963.
- [81] M. Mondello and N. Goldenfeld, Phys. Rev. A 42 (1990) 5865.
- [82] N. Shvartsman and I. Freund, Phys. Rev. Lett. 72 (1994) 1008; Phys. Rev. Lett. 72 (1994) 4156 (E).
- [83] G. Grinstein, private communication.

Figure 1: Snapshot of a 70×70 region. This is $\sim 1/12$ of the total area of the simulation. The solid lines are where $\text{Re}[A] = 0$, and the dashed lines are where $\text{Im}[A] = 0$. Filled circles (\bullet) are vortices with topological charge $+1$, and the open circles (\circ) have charge -1 . The typical distance between defects is 10. This picture is for $c = 1.5$, $b_x = -0.75$, and $b_y = -3.0$.

Figure 2: $\text{Re}[\langle A^*(\mathbf{r})A(0) \rangle]$ averaged over 12 different systems with $L_x = L_y = 240$. The solid line is for $\mathbf{r} = r\hat{x}$ while the dashed line is for $\mathbf{r} = r\hat{y}$.

Figure 3: $\langle S(k_x) \rangle = \text{Re}\langle A^*(k_x)A(0) \rangle$ averaged over 500,000 time steps, with parameter values $c = 1.5$, $b_x = -1.5$, and $b_y = -1.5$. The system has size $L_x = L_y = 60$ with 90 Fourier modes in each direction. Other Fourier modes show similar behavior.

Figure 4: $\text{Prob}(\text{Re}[A(x)])$ averaged over space at a particular time (solid line) and over time at a particular spatial location (dashed line). The spatial average is over 129,600 points, while the time average is over 200,000 time steps. This is for $c = 1.5$, $b_x = -0.75$, and $b_y = -3.0$.

Figure 5: $\text{Prob}(|A(x)|)$ averaged over space at a particular time (solid line) and over time at a particular spatial location (dashed line). The spatial average is over 129,600 points, while the time average is over 200,000 time steps. Note that values of $|A| > 1.0$ represent shocks in the system, while the nonzero values at the limit $|A| = 0$ represent the defects in the system. This is also for $c = 1.5$, $b_x = -0.75$, and $b_y = -3.0$.

Figure 6: $\text{Prob}(\text{Re}[A(k_x)])$ averaged over 500,000 time steps, with parameter values $c = 1.5$, $b_x = -1.5$, and $b_y = -1.5$. Also shown in the dashed line is a Gaussian with mean 0 and standard deviation 0.08 for comparison. We have chosen a value of $k = \frac{2\pi(2)}{60}$. The system has size $L_x = L_y = 60$ with 90 Fourier modes in each direction.

Figure 7: $\text{Prob}(n)$. This was obtained from a time series of length 70,000 time steps. This is for a system of size $L_x = L_y = 240$ with 360 Fourier modes in each direction. The parameter values are $c = 1.5$, $b_x = -0.75$, and $b_y = -3.0$. The dashed line is the exponential with mean $\mu = 422.8$ and $\sigma^2 = 397$.

Figure 8: $G_\rho(\mathbf{r})$ versus r . The solid line is for the \hat{x} direction, while the dashed line is for the \hat{y} direction. Also shown is a line for $G = 0$. Note that G attains its asymptotic limit of 0 from different sides of this line. The parameters are $c = 1.5$, $b_x = -0.75$, and $b_y = -3.0$.

Figure 9: $|G_\rho(\mathbf{r})|$ versus r (linear-log plot). The parameters are $c = 1.5$, $b_x = -0.75$, and $b_y = -3.0$.

Figure 10: Log–log plot of $|G_\rho(\mathbf{r})|$ versus r . The solid line corresponds to the \hat{x} direction and the dashed line to the \hat{y} direction. Also shown is a line with slope that would correspond to $|G_\rho(r)| \sim 1/r^2$. The parameters are $c = 1.5$, $b_x = -0.75$, and $b_y = -3.0$.

Figure 11: Log–log plot of $|G_\rho(\mathbf{r})|$ versus r for the case where we have added a term $d\partial_x A(x, t)$ to the complex Ginzburg–Landau equation. Here we have $d = 0.1$. The solid line corresponds to the \hat{x} direction and the dashed line to the \hat{y} direction. Also shown is a line with slope that would correspond to $|G_\rho(r)| \sim 1/r^2$. The parameters are $c = 1.5$, $b_x = -0.75$, and $b_y = -3.0$.

Figure 12: Log–log plot of $|G_\rho(\mathbf{r})|$ versus r for the case where we have added a term $d\partial_x^3 A(x, t)$ to the complex Ginzburg–Landau equation. Here we have $d = 0.1$. The solid line corresponds to the \hat{x} direction and the dashed line to the \hat{y} direction. Also shown is a line with slope that would correspond to $|G_\rho(r)| \sim 1/r^2$. The parameters are $c = 1.5$, $b_x = -0.75$, and $b_y = -3.0$.

Figure 13: Log–log plot of $|G_\rho(\mathbf{r})|$ versus r for the case where we have added a term $d\partial_x |A(x, t)|^2 A(x, t)$ to the complex Ginzburg–Landau equation. Here we have $d = 1.0$. The solid line corresponds to the \hat{x} direction and the dashed line to the \hat{y} direction. Also shown is a line with slope that would correspond to $|G_\rho(r)| \sim 1/r^2$. The parameters are $c = 1.5$, $b_x = -0.75$, and $b_y = -3.0$.

Figure 14: Log–log plot of $|G_\rho(\mathbf{r})|$ versus r for the case where we have added a term $d\partial_x^3 |A(x, t)|^2$ to the complex Ginzburg–Landau equation. Here we have $d = 1.0$. The solid line corresponds to the \hat{x} direction and the dashed line to the \hat{y} direction. Also shown is a line with slope that would correspond to $|G_\rho(r)| \sim 1/r^2$. The parameters are $c = 1.5$, $b_x = -0.75$, and $b_y = -3.0$.

Figure 15: Correlation function of the coarse–grained topological order parameter. The coarse graining scale is $\sigma = 10$. The parameters are $c = 1.5$, $b_x = -0.75$, and $b_y = -3.0$.

Figure 1

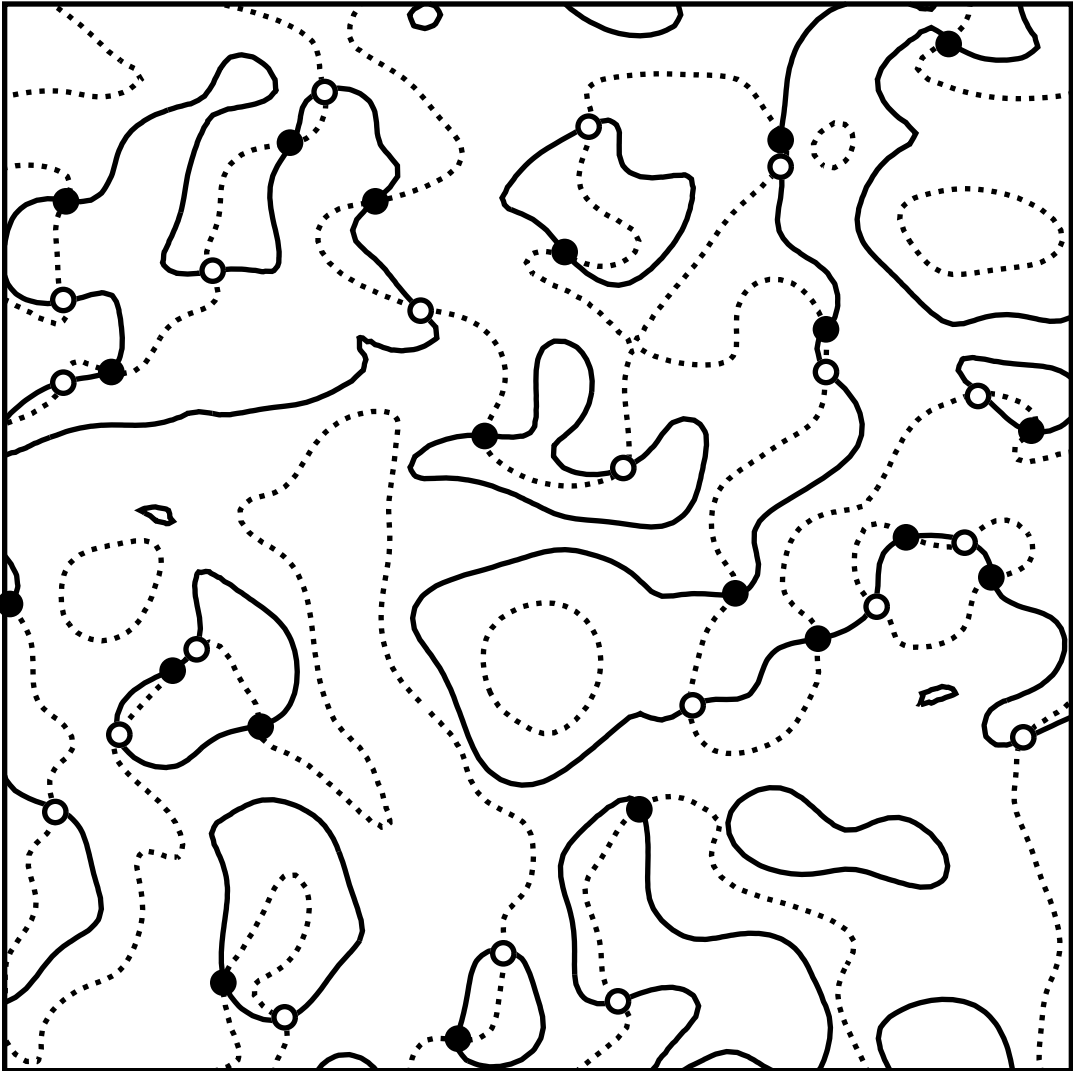


Figure 2

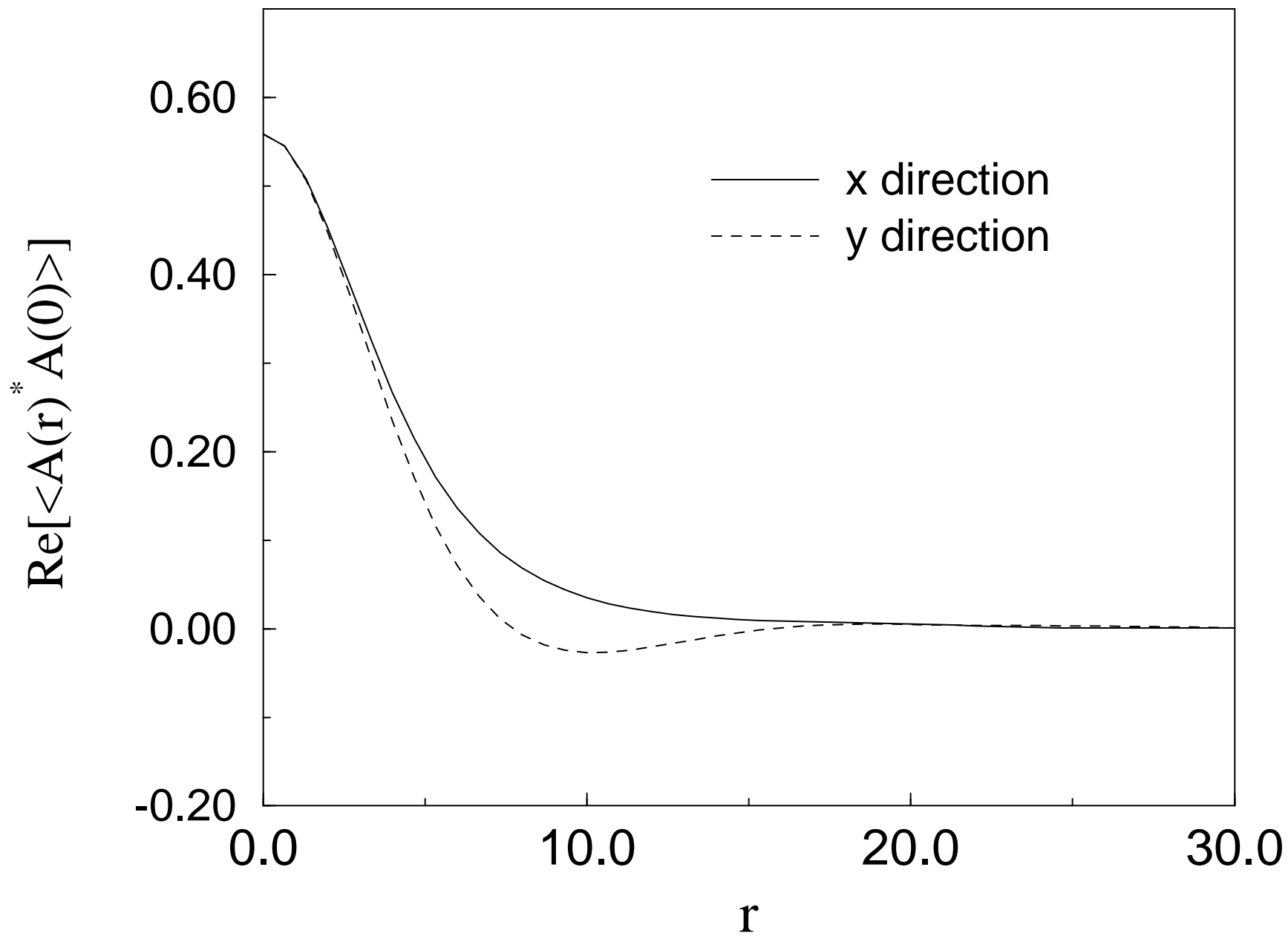


Figure 3

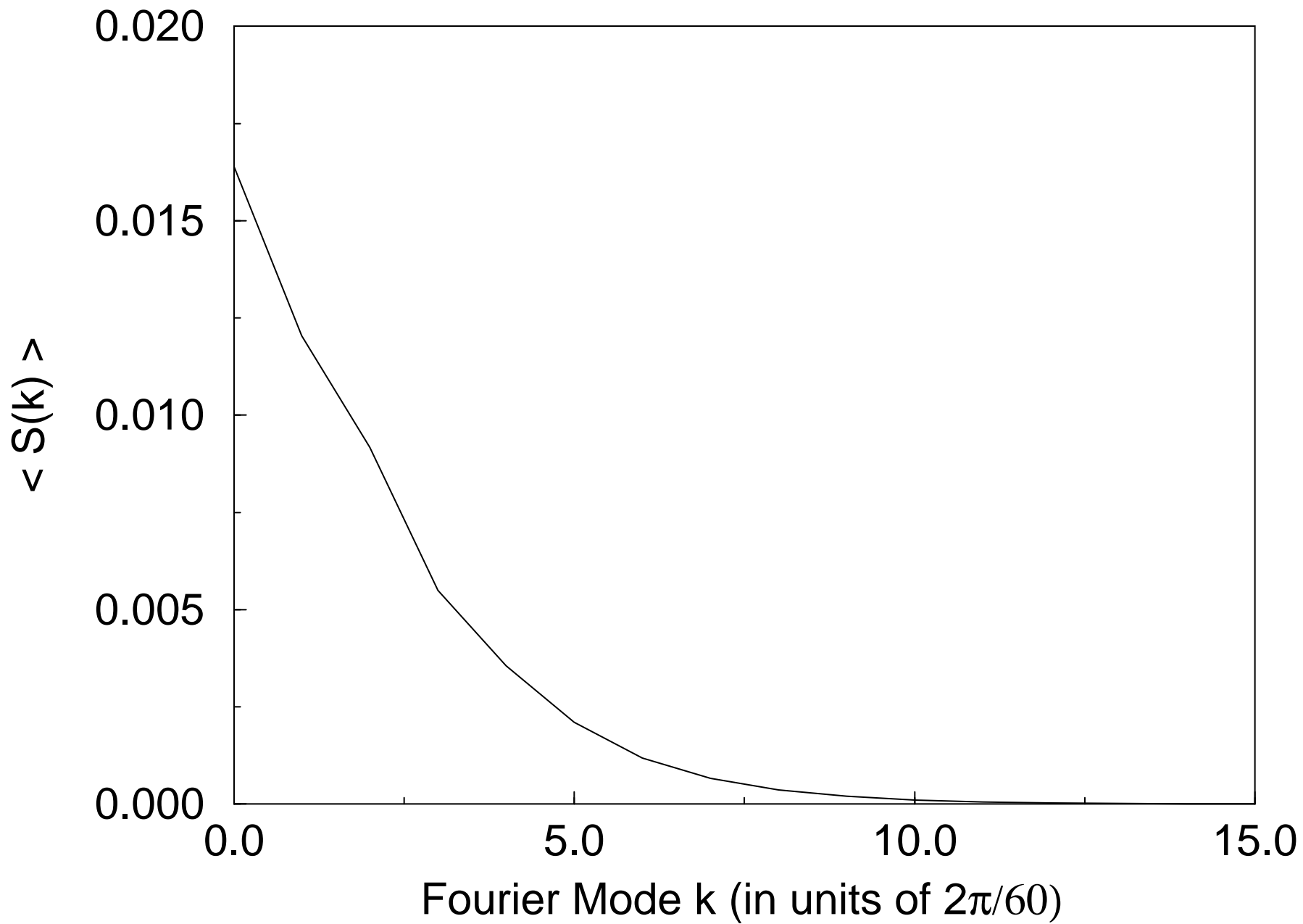


Figure 4

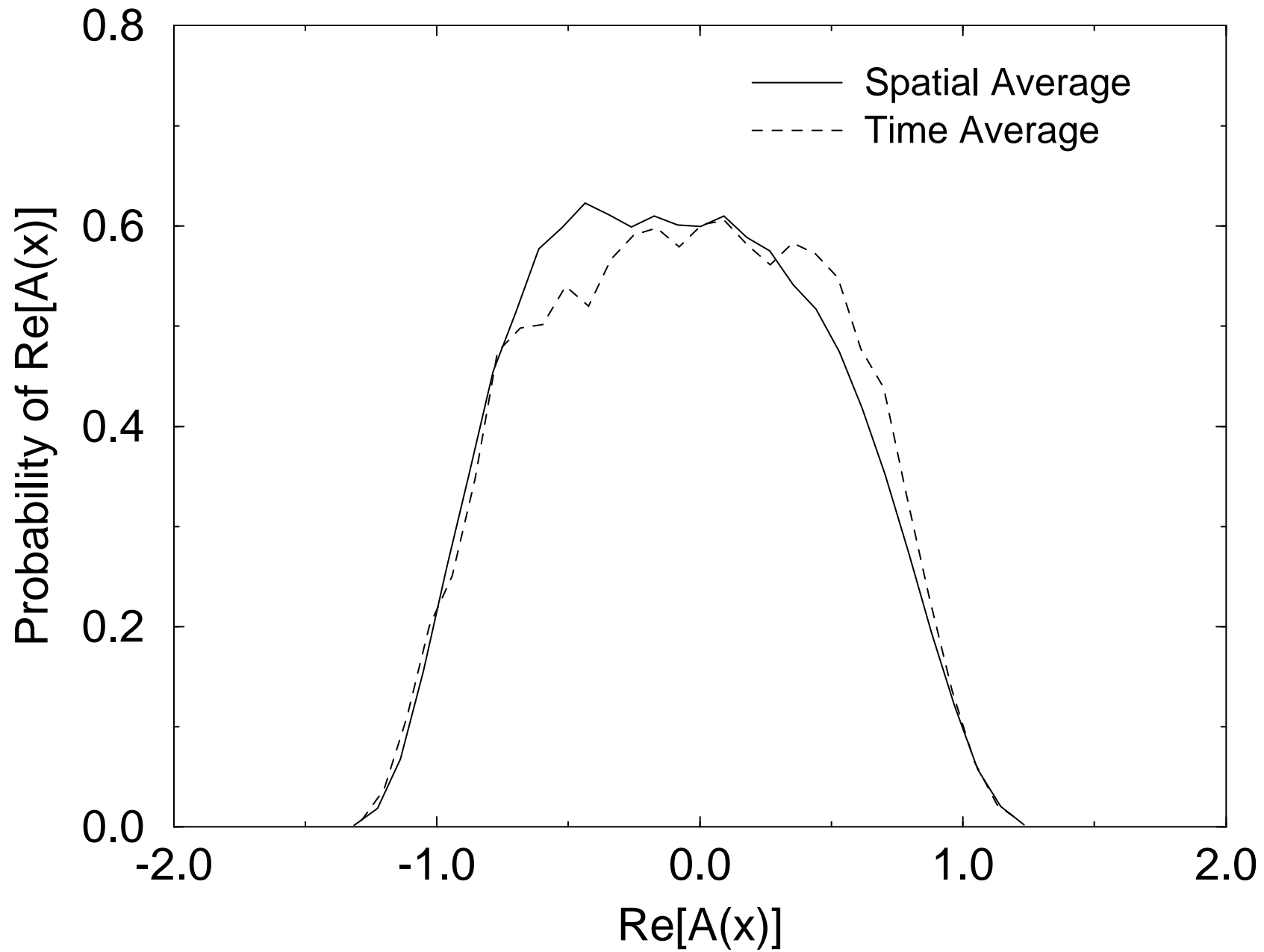


Figure 5

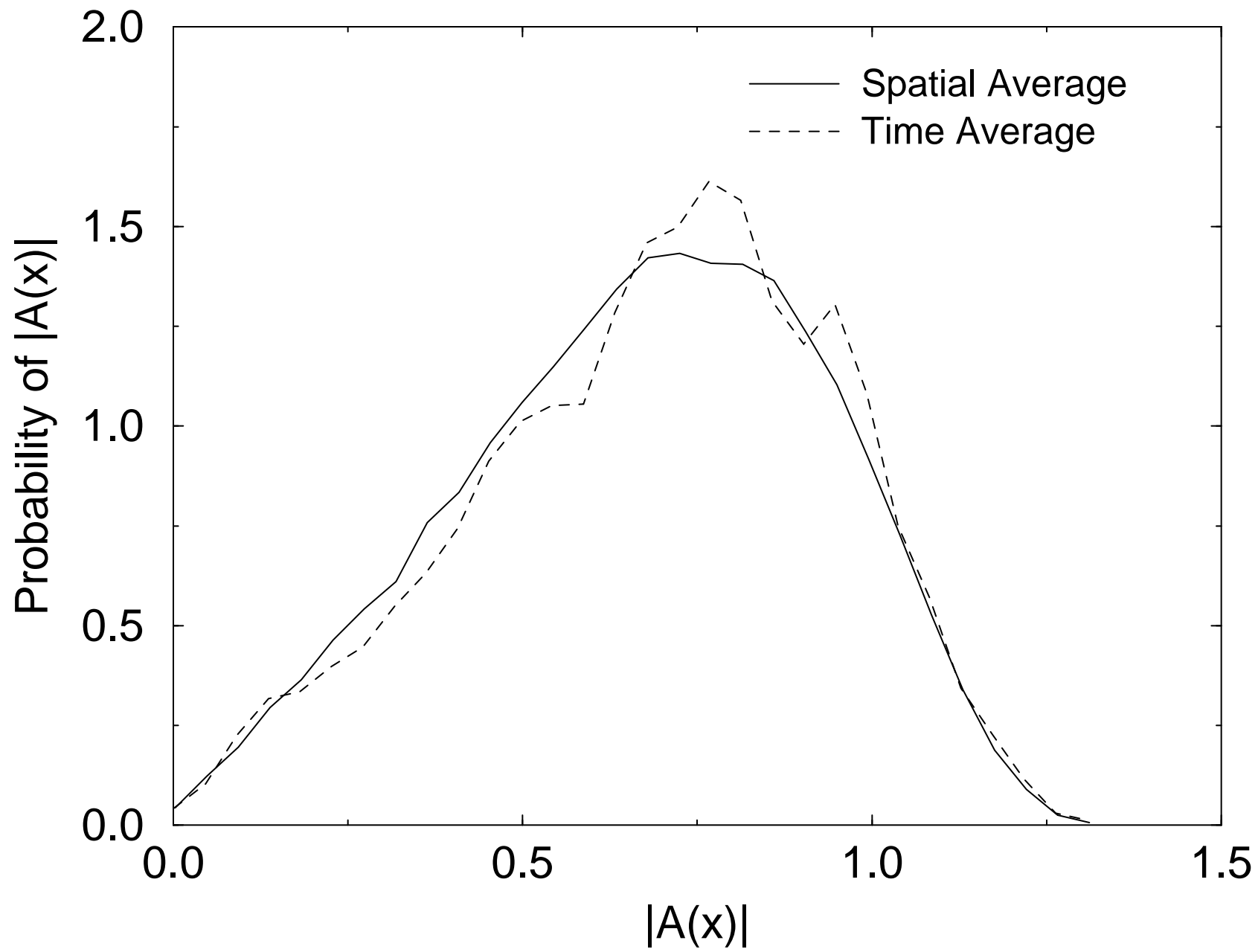


Figure 6

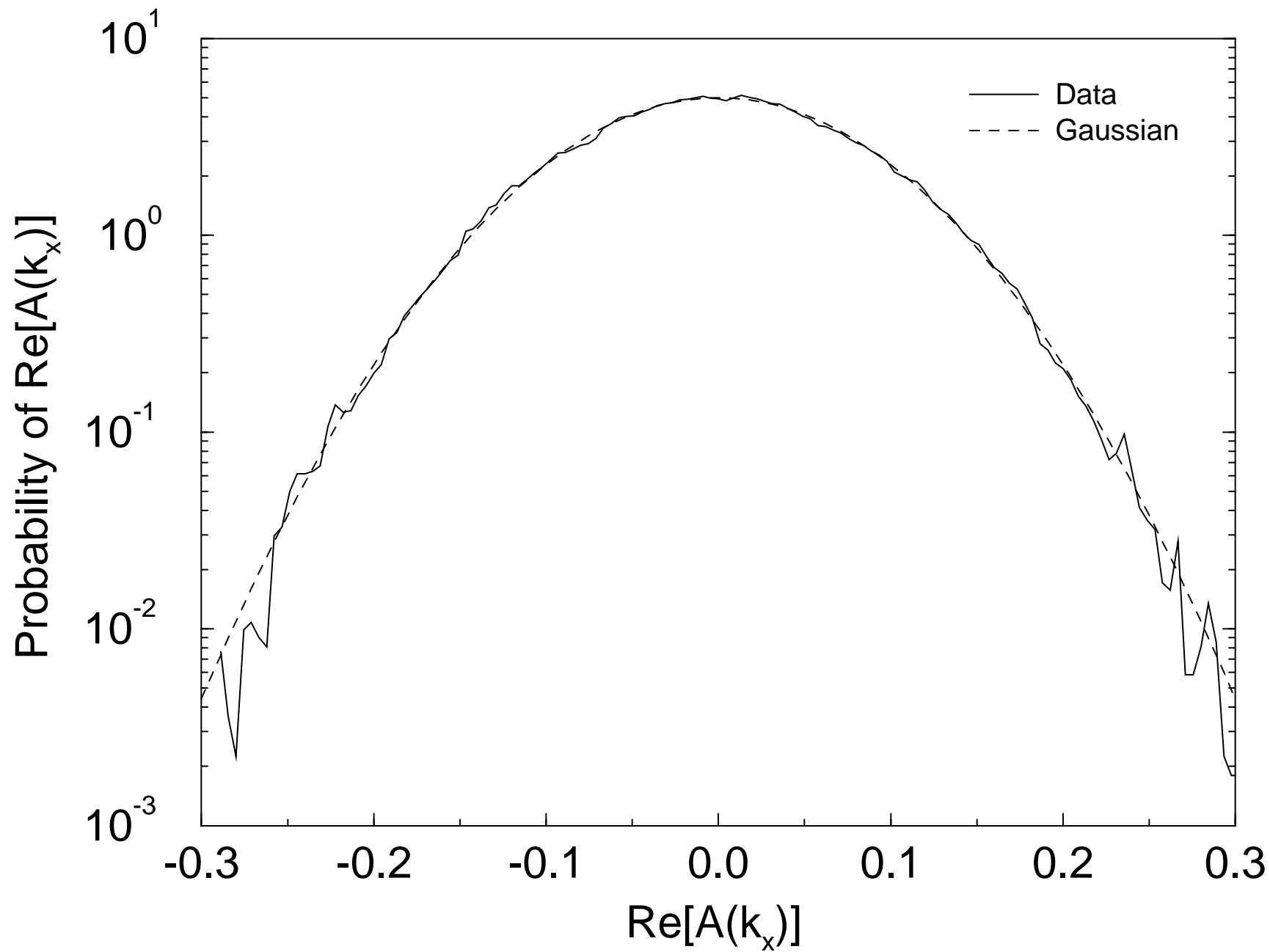


Figure 7

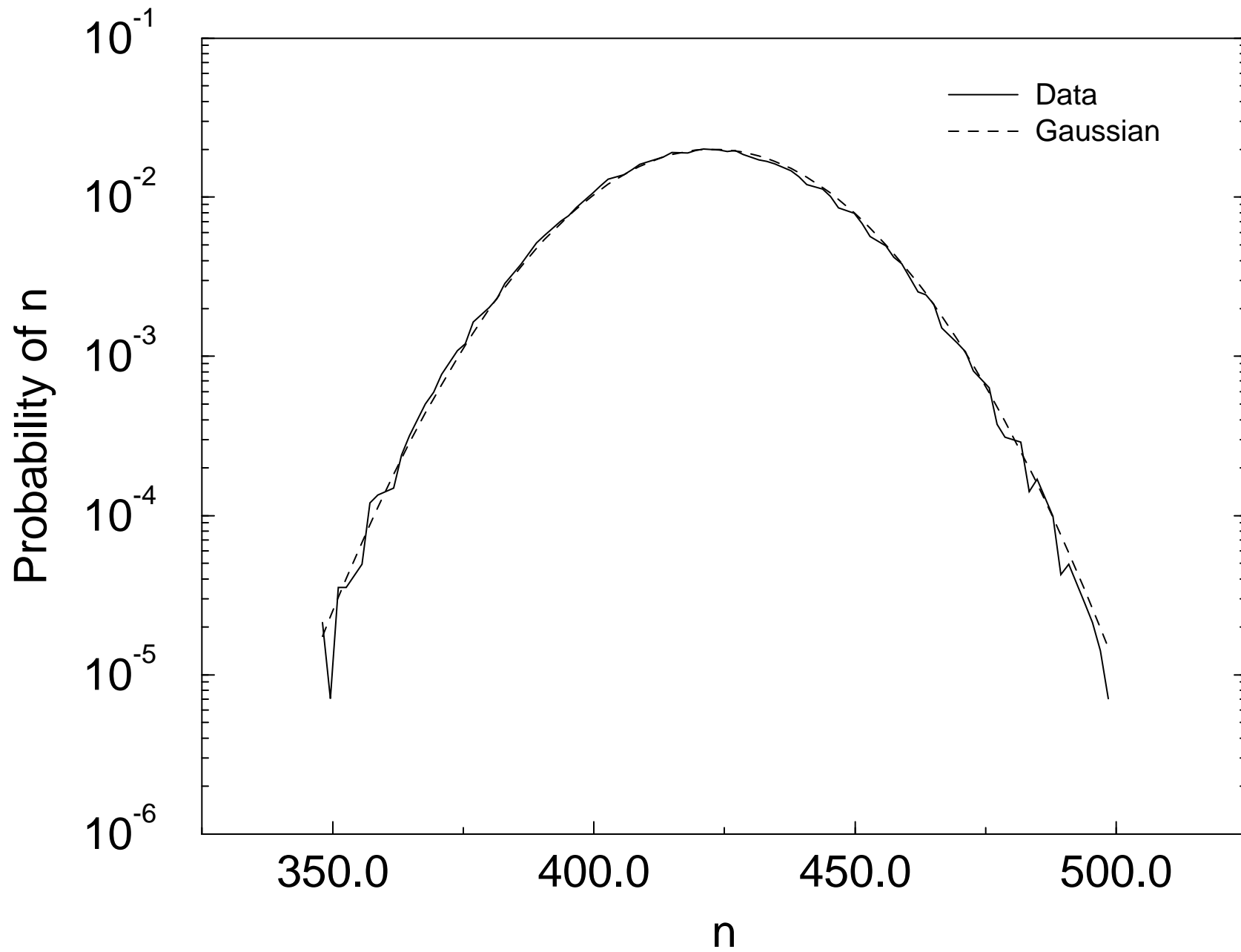


Figure 8

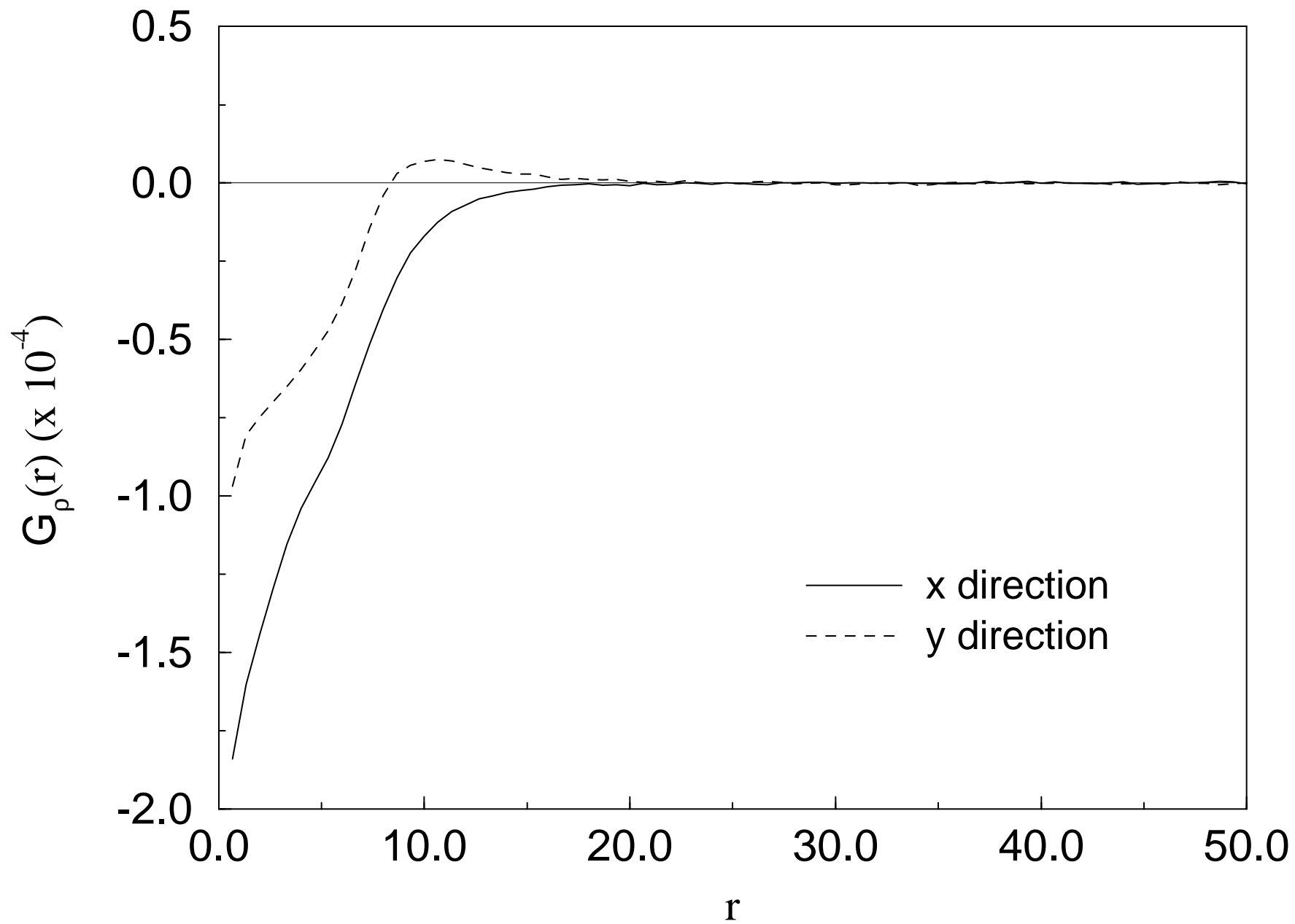


Figure 9

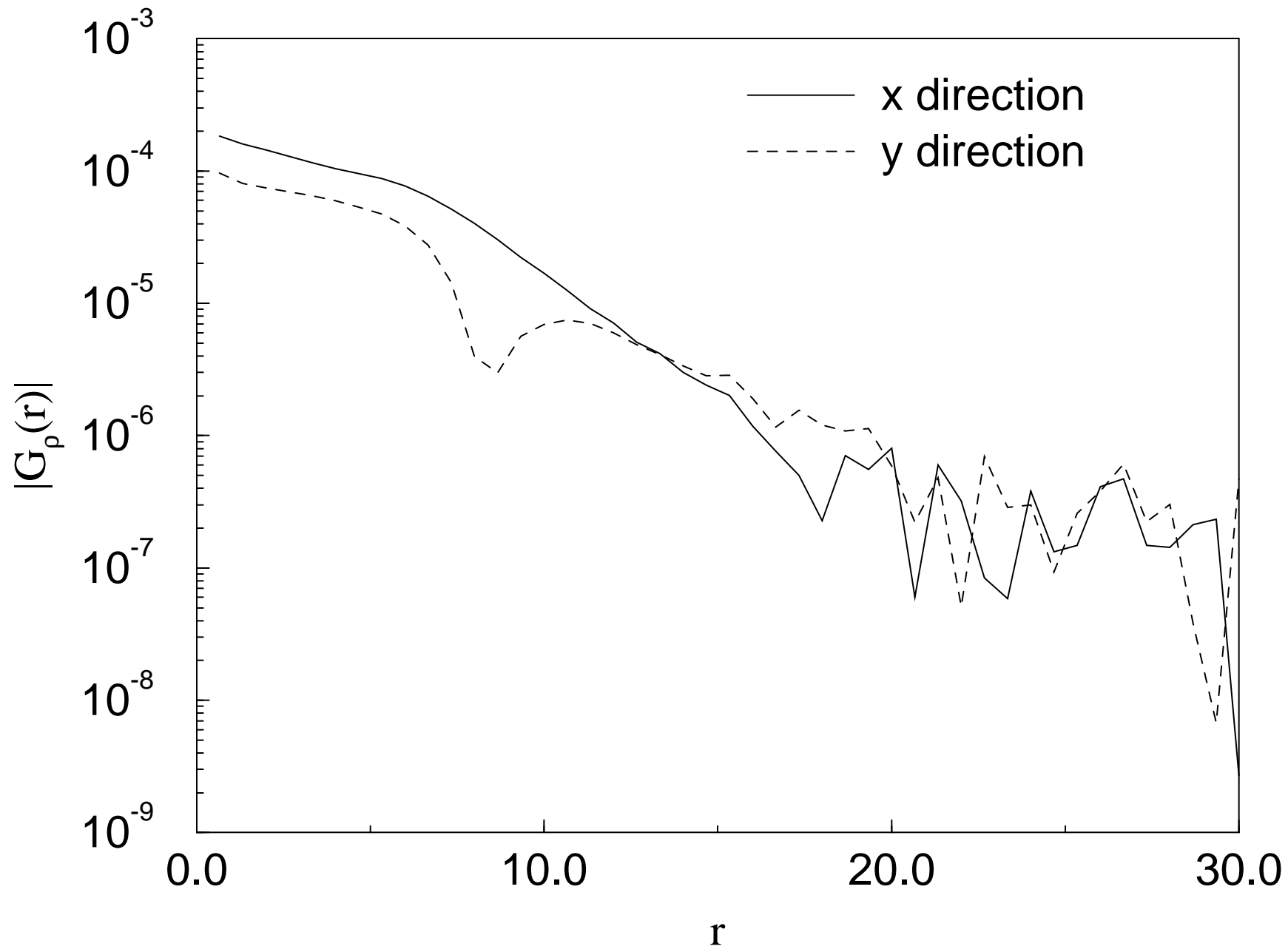


Figure 10

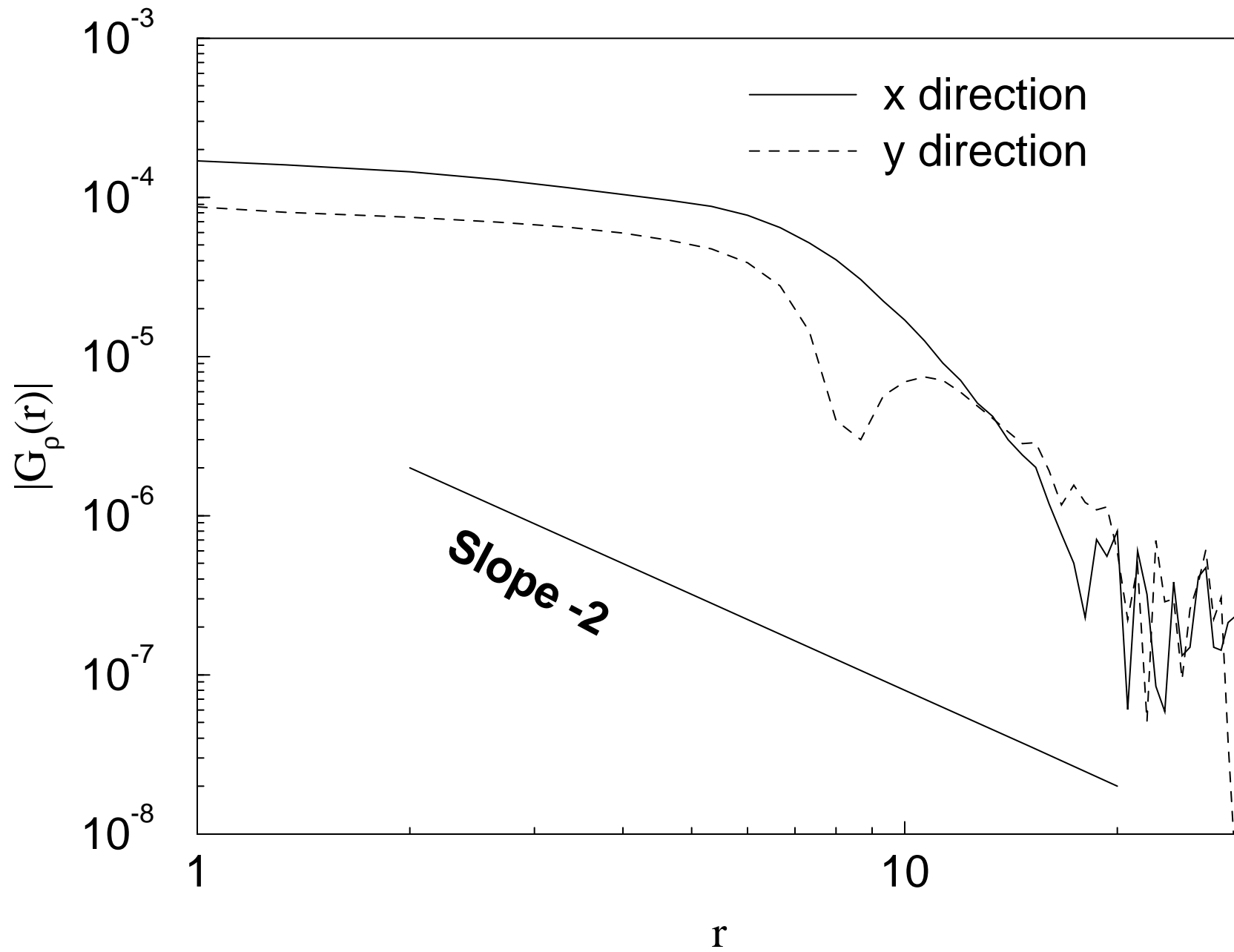


Figure 11

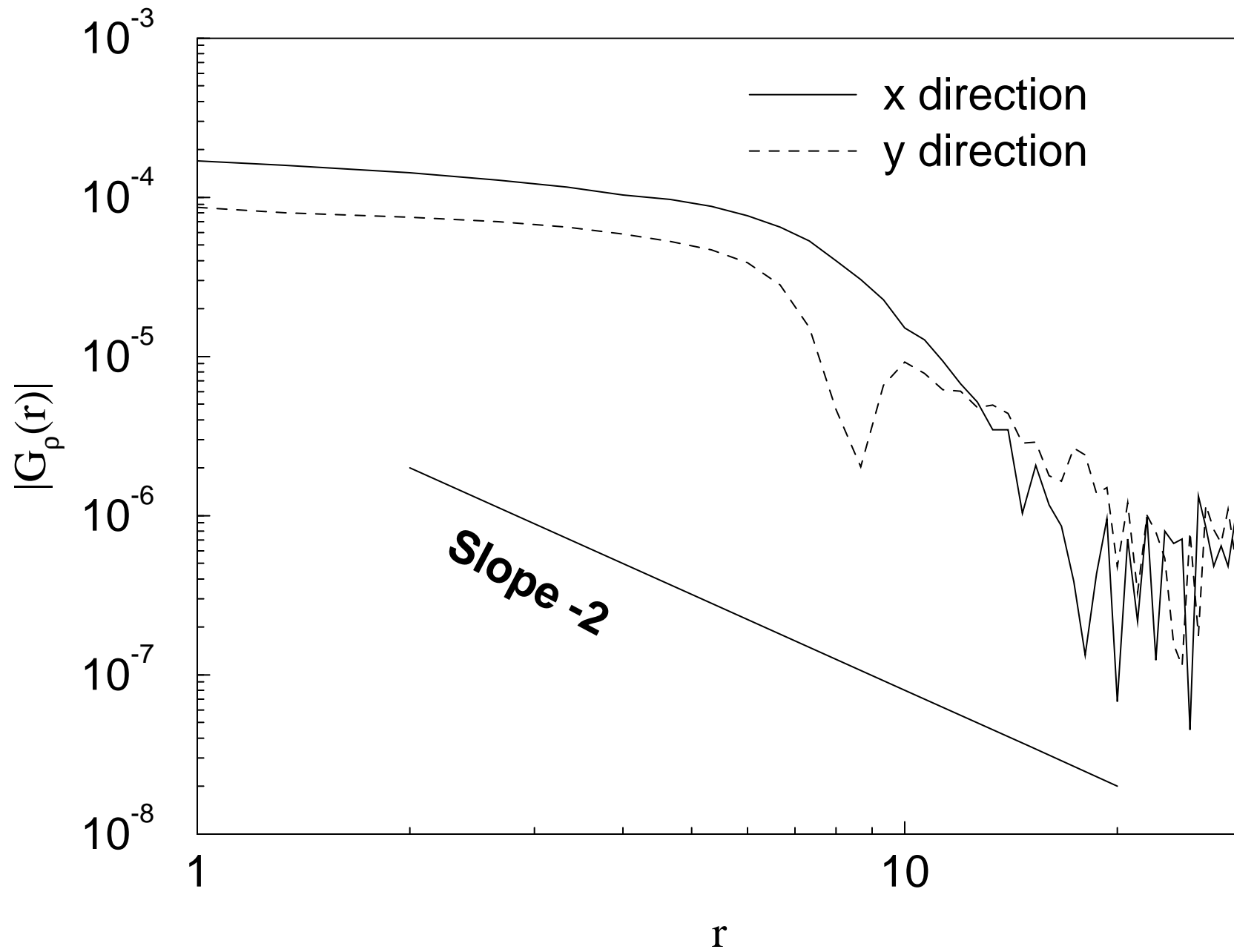


Figure 12

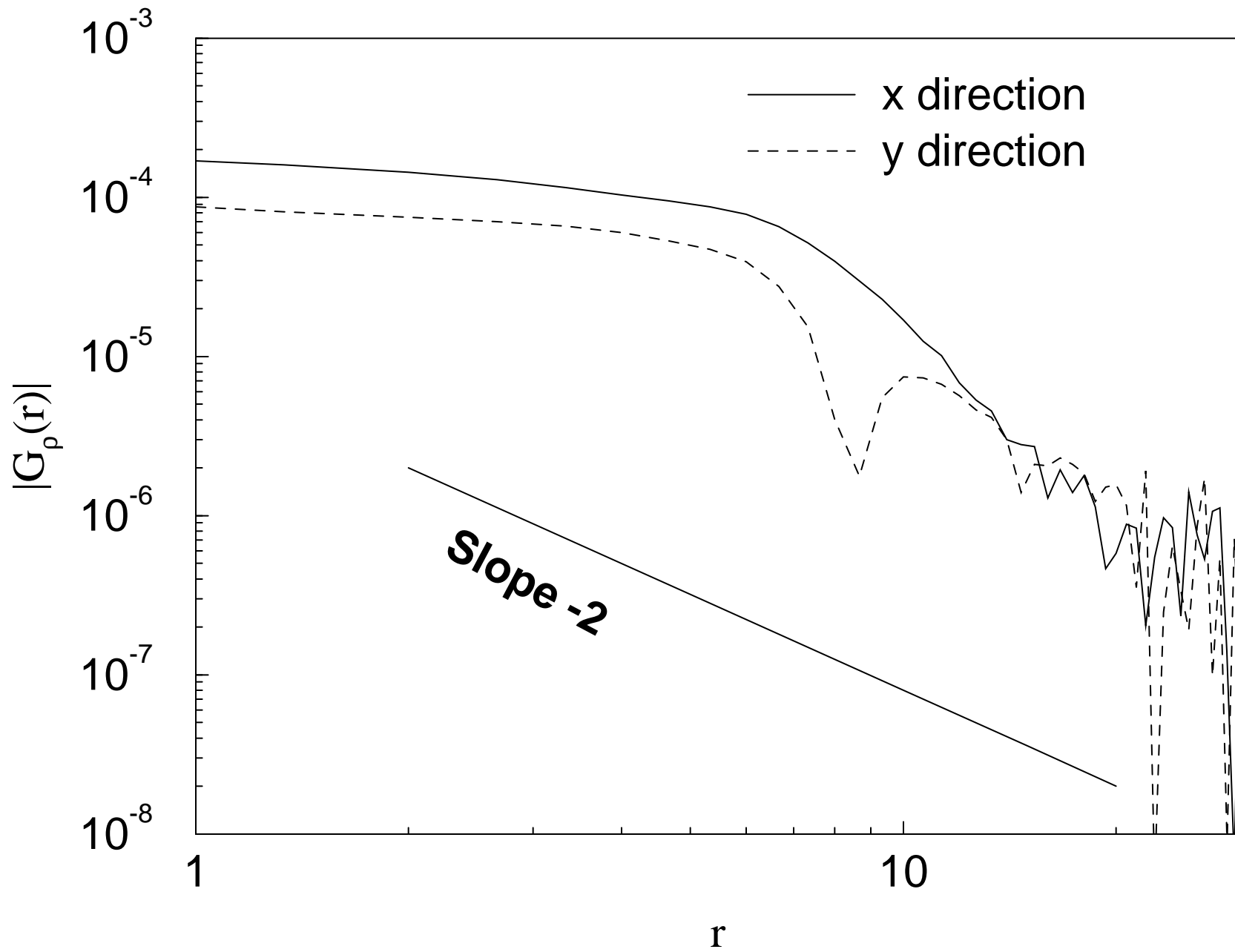


Figure 13

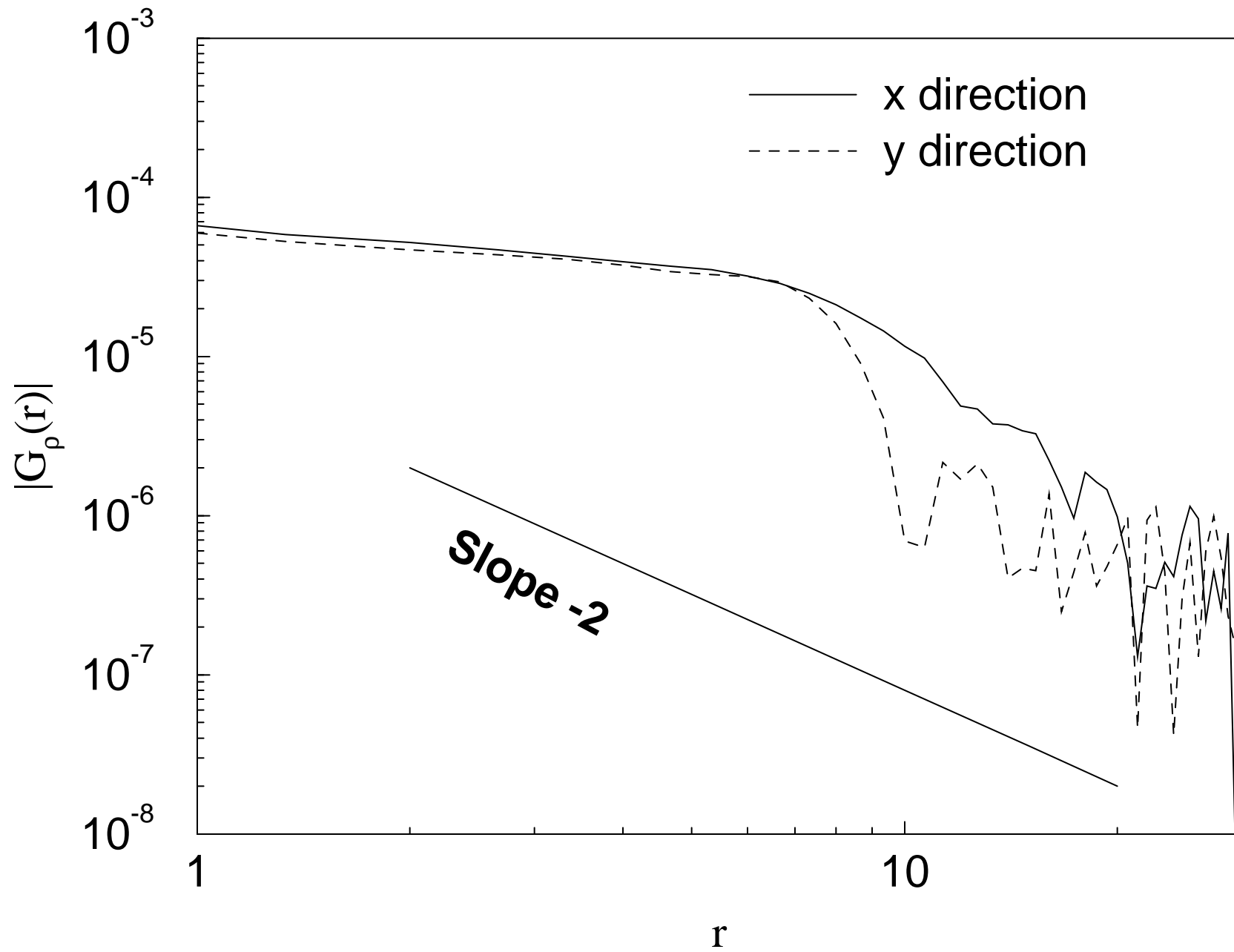


Figure 14

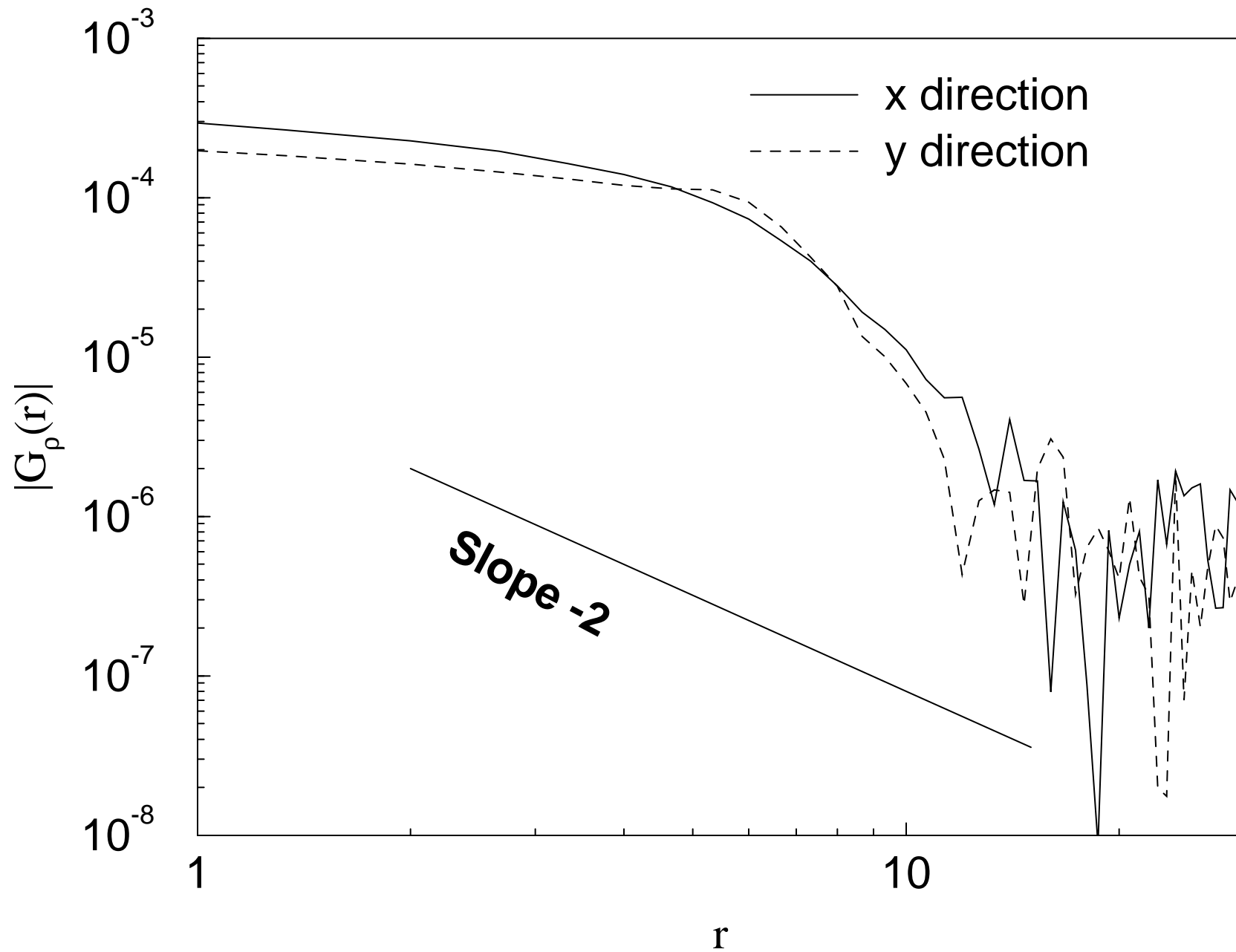


Figure 15

